Christopher Domes, BSc

The role of ATGL in muscle cell differentiation and metabolism

MASTERARBEIT

zur Erlangung des akademischen Grades

Master of Science

Masterstudium Biochemie und Molekular Biomedizin

eingereicht an der

Technischen Universität Graz

Betreuerin

Priv.-Doz. Mag. Dr. Martina Schweiger

Institut für Molekulare Biowissenschaften

Karl-Franzens Universität Graz

Graz, August, 2016

EIDESSTATTLICHE ERKLÄRUNG

Ich erkläre an Eides statt, dass ich die vorliegende Arbeit selbstständig verfasst, andere als die angegebenen Quellen/Hilfsmittel nicht benutzt, und die den benutzten Quellen wörtlich und inhaltlich entnommenen Stellen als solche kenntlich gemacht habe. Das in TUGRAZonline hochgeladene Textdokument ist mit der vorliegenden Masterarbeit identisch.

Datum

Unterschrift

Acknowledgement

First of all, I would like to express my deep sense of gratitude to my supervisor Martina Schweiger for her committed support and the pleasant working atmosphere. She provided me with the possibility to learn many scientific methods and experience the academic modus vivendi. Furthermore she allowed me to be part of a successful group which upholds the ambition to reputably expand the scientific knowledge.

I would also like to express my sincere thanks to the people of the whole Zechner lab. Their irreplaceable assistance during my lab work allowed me to perform my sophisticated experiments. In addition I would like to thank all people of the Haemmerle, Lass and Zimmermann lab for the great camaraderie at the institute. The professional climate facilitated me to improve my skills in an enjoyable environment.

Finally, I want to give my biggest thanks to my parents Bruno and Edith. I am very grateful that they gave me the opportunity to pursue my academic interests. I will always remember thankfully their unconditional endorsement. At this point I would also like to thank my sister Ann-Katrin for her fantastic support with all the challenges I faced.

Abstract

ATGL is a key enzyme in neutral lipolysis, the process which provides free fatty acids by the breakdown of stored triglycerides. Mutations in the *ATGL*-gene are known to cause neutral lipid storage disease with myopathy (NLSDM) which is associated with several symptoms. A pronounced condition appearing in NLSDM patients is the appearance of intramuscular fat and the loss of skeletal muscle accompanied by progressing muscle weakness. The mechanism responsible for muscle atrophy is subject of current studies.

First, we wanted to investigate whether ATGL deficiency impairs muscle cell differentiation, hence leading to insufficient supply of myofibers. Therefore, we applied ATGL gene silencing in a mouse myoblast cell line (C2C12). The performed differentiation studies in cell culture revealed that the decrement of physiological ATGL concentrations had no negative impact on myogenic differentiation of C2C12 cells. We furthermore intended to analyze the consequences of ATGL deficiency ex vivo in primary muscle stem cells of ATGL knockout mice. Therefore, we established a protocol for the isolation of primary cells. We succeeded in isolating and differentiating cells of wild-type, but unfortunately due to the lack of time and mice were not able to isolate cells from ATGL knockout mice. Since ageing is associated with muscular disorders, our second approach was to study the role of ATGL in muscle atrophy during ageing. Therefore, we wanted to elucidate whether old mice constitute a model for muscle damage. Hence, we analyzed muscle tissue for atrophy markers and fat accumulation. Interestingly, our results indicated that old mice possess healthy muscles without signs of degeneration, making them an invalid model to study ageing associated muscle atrophy. To overcome this obstacle, we performed glycerol injections into mouse muscles expecting muscle damage to occur, associated with the formation of intramuscular fat. We hypothesized that ATGL deficiency leads to impaired muscle regeneration and enhanced formation of adipocytes. However, we were not able to induce adipocyte formation in murine muscle.

Taken together, our results indicate that ATGL is not mandatory for the differentiation of C2C12 myoblasts to myocytes. We successfully established a protocol for the isolation and differentiation of primary myoblasts. Moreover, we found that 19-month-old mice do not show signs of muscle atrophy and hence are not suited to study ageing induced sarcopenia.

Table of Contents

1 Introduction

1.1 ATGL - a key player in neutral lipolysis

Constant energy supply in mammals is warranted by a storing technique that incorporates triacylglycerols (TG) into intracellular lipid droplets (LD). During nutritional opulence LDs are stacked with hydrophobic TGs from food due to the process of lipogenesis. In times of nutritional deprivation and upon high energy demand, lipolysis releases energy-rich metabolites by the breakdown of stored TGs to fuel the organism (reviewed in (1)).

1.1.1 The lipolytic cascade in triacylglycerol catabolism

LD organelles filled mainly with TGs occur in almost all cell types, but are most abundant in adipocytes of adipose tissue (AT) (2). Besides TGs, the hydrophobic core in LDs consists of steryl esters (SE) in varying compositions, depending on the kind of cell (3). The phospholipid monolayer surrounding the aggregated lipids is associated with proteins especially of the perilipin family (2; 4). These perilipins, together with further proteins, stabilize the LD structure and regulate the TG breakdown. In fact, during lipolysis perilipins are crucial in governing enzymes that perform lipid hydrolysis in a cascade-like fashion, incrementally releasing free fatty acids (FFA) (Figure 1) (1). In general, adipose triglyceride lipase (ATGL) hydrolyses TG, producing one molecule diacylglycerol (DG) and one free fatty acid (FFA) (1). Subsequently, hormone sensitive lipase (HSL) cleaves off a second fatty acid residue, leading to a monoacylglycerol (MG) molecule (1). Finally, monoacylglycerol lipase (MGL) hydrolyzes MG into glycerol, releasing the third FFA (1).

The expression of ATGL, the first enzyme in the lipolytic cascade is upregulated by fasting, glucocorticoids and peroxisome proliferator-activated receptor (PPAR) agonists (5; 6). Upon food intake and increased insulin levels the expression is downregulated (7). To gain full activity, ATGL has to be stimulated by its activator protein comparative gene identification-58 (CGI-58), also known as α/β-hydrolase domain-containing protein 5 (ABHD5) (8). Increasing hydrolysis of TGs up to 20-fold, CGI-58 itself seems incapable of performing hydrolytic enzyme reactions, despite an existing α/β hydrolase domain (8). This is in part due to the presence of an

asparagine instead of a catalytically active serine residue in the active site (9). More recently, a protein was identified that acts as counterpart to CGI-58 by inhibiting ATGL (10). G0G1 switch protein 2 (G0S2) contains a hydrophobic domain that is able to bind the patatin-like domain of ATGL (10). The interaction occurs independently of CGI-58 and results in an enzymatic inhibition (11).

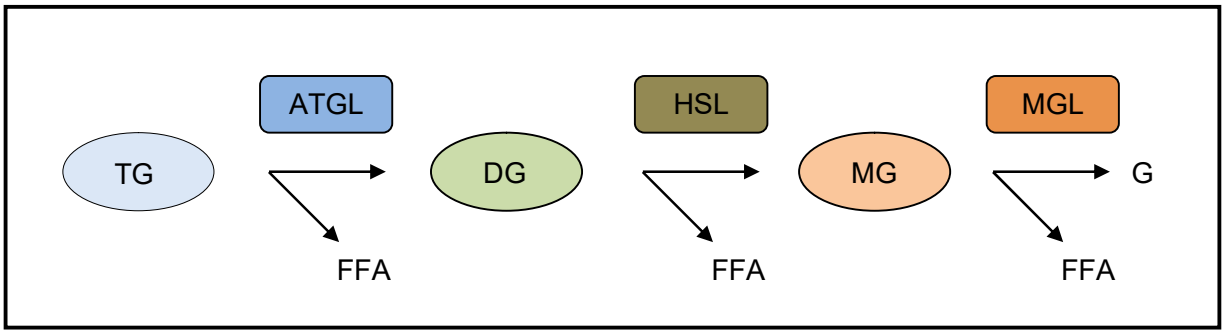

Figure 1: The intracellular lipolytic cascade with participating enzymes and molecules. Abbreviations: ATGL, adipose triglyceride lipase; DG, diaclyglycerol; FFA, free fatty acid; G, Glycerol; HSL, hormone-sensitive lipase; MG, monoacylglycerol; MGL, monoacylglycerol lipase; TG, triacylglycerol.

The fundamental process depicted in Figure 1 exemplifies the common scheme for the breakdown of TGs, however, the actual regulatory mechanism differs between adipose tissue and oxidative tissues (reviewed in (7)). In adipose tissue, CGI-58 is bound to perilipin-1 (Plin1) under unstimulated conditions and thereby localized to LDs (12). As a result, the activity of ATGL is low. β-adrenergic signaling leads to the activation of protein kinase A (PKA) (7). Subsequently, multiple phosphorylation of Plin1 performed by PKA enables CGI-58 to dissociate and interact with ATGL (13; 14). Thereby the system is shifted towards a stimulated state and the hydrolytic activity of ATGL increases. Besides Plin1, activated PKA also phosphorylates HSL, boosting the hydrolysis of DGs (15). To maintain full activity, HSL has to be bound by phosphorylated Plin1, which mediates LD association (16; 17; 18). MGL, the last enzyme in the lipolytic cascade is a member of the α/β hydrolase fold protein family (1). In addition to its pivotal role in hydrolysis of lipopytic MGs, MGL is an important regulator in endocannabinoid signaling by inactivating 2-arachidonoylglycerol (7). The mechanism regulating MGL activity is still under investigation.

In oxidative tissues like skeletal muscle, Plin1 is substituted by Plin5 (7). Plin5 is upregulated under fasting conditions and binds ATGL and CGI-58 (19; 20). This complex brings the proteins in close vicinity and allows them to interact (21). Since Plin5 localizes to LDs, it concentrates ATGL and CGI-58 at their place of action, resulting in increased TG hydrolysis (21). Because of the lack of Plin1 in oxidative tissue like skeletal muscle, a currently unknown mechanism is required to associate HSL with LDs. The activation of HSL is carried out by phosphorylation through PKA upon β–adrenergic stimulation and muscular exercise (22).

It is now well established that FFAs released during lipolysis fulfill more functions than powering the organism through mitochondrial β-oxidation. FFAs provide ligands and ligand precursors for nuclear receptor transcription factors (TF), which regulate the expression in a variety of genes (7). Important lipid-activated TFs are the members of the PPAR family, which regulate genes in metabolic processes like lipogenesis, lipolysis and oxidative phosphorylation (7). Haemmerle and colleagues could show that impaired lipid signaling in ATGL knockout mice led to decreased expression of genes regulated by PPARα (23). ATGL knockout mice displayed severe cardiac lipid accumulation and mitochondrial dysfunction leading to cardiomyopathy due to reduced liberation of PPARα ligands by ATGL (23). Furthermore, Schreiber and colleagues showed that ATGL deficiency also leads to impaired PPARγ signaling, influencing lipogenesis in white adipose tissue (24).

1.1.2 Adipose triglyceride lipase (ATGL)

For a long time it was thought that HSL besides its activity towards DGs, also performs the first step in neutral lipolysis by hydrolyzing TGs. In 2004, the discovery of a new lipase was reported independently by three scientific groups (5; 25; 26). Due to its localization and action, the identified protein was named adipose triglyceride lipase (ATGL) (25). Furthermore, the enzyme is known as desnutrin (5), phospholipase A2ζ (26) and by its official name patatin-like phospholipase domain-containing protein A2 (PNPLA2) (27). It has now been established, that ATGL hydrolyzes TGs into DGs and FFAs, but does not show significant activity for MGs, DGs or SEs (25). Additionally, DG transacylase (26) and phospholipase (28) activity was detected to a minor extent in ATGL, but the physiological implications are still a subject of investigation.

ATGL belongs to the patatin-like phospholipase domain containing protein family (27). A hallmark of this family is the patatin-like domain which is located at the N-terminus of ATGL (PNPLA2) (27). The patatin-like domain contains a Ser-Asp catalytic dyad and a conserved

GXSXG lipase motif (29). According to mutation studies, the catalytic serin 47 within the active site is crucial for the physiological function of the hydrolase (30). A hydrophobic stretch located to the C-terminal region is reported to be relevant in regulating enzyme activity and the association of ATGL with LDs (31; 32).

The *ATGL*-gene, expressed in virtually all tissues (5; 25; 33; 34), is annotated as *PNPLA2* in human and *Pnpla2* in mouse encoding for an mRNA of 2.4 kb and 2.6kb respectively and a 504 amino acid protein of 55 kDa in humans and a 486 amino acid protein of 54 kDa in mice (1). The highest gene expression was reported in white and brown adipose tissue, followed by testis, cardiac- and skeletal muscle (25).

The importance of ATGL is evidenced in mice, where the enzyme has been genetically deleted (ATGL knockout). These mice show TG accumulation in almost all tissues and thus have increased body fat (35). Furthermore they suffer from severe cardiomyopathy leading to an early death about 12 weeks after birth (35). Mutations in the human *ATGL*-gene cause symptoms, similar to those of ATGL knockout mice, which are characteristics of neutral lipid storage disease with myopathy (NLSDM) (see1.1.3).

1.1.3 Mutations in the *ATGL*-gene lead to severe diseases

The importance of sufficient ATGL activity was first recognized, when ATGL knockout mice where characterized, displaying an unhealthy phenotype with a short lifespan (35). Characterization of patients suffering from lipid storage abnormalities with various symptoms revealed that humans are also affected by disturbed lipolytic capacity due to insufficient ATGL activity (reviewed in (36)).

During early studies of diseases characterized by abnormal neutral lipid accumulation in several tissues, two distinct phenotypes became apparent. Besides commonly shared lipid-filled vacuoles in most tissue cells, some patients showed symptoms of a skin barrier defect called ichthyosis, whereas other patients showed severe myopathy in heart- and skeletal muscle (37). At first, these conditions where subsumed under the name neutral lipid storage disease (NLSD) (38). Associated with the disease are lipid filled vacuoles in leukocytes, known as Jordans' anomaly, which can be used as diagnostic tool (39). Patients suffering from NLSD exhibit perturbed lipolysis due to inadequate hydrolysis of stored TGs. Further genetic analysis showed that the autosomal recessive disorder is caused by independent mutations in two genes.

Whenever mutations in the *PNPLA2*-gene occur, patients develop myopathy symptoms (40). Therefore this disorder was classified as neutral lipid storage disease with myopathy (NLSDM). Whenever mutations in the gene encoding for CGI-58 arise, patients suffer from a skin defect called ichthyosis (9). Congruously this disorder was classified as neutral lipid storage disease with ichthyosis (NLSDI).

Until now, approximately 44 patients are reported to suffer from NLSDM caused by different mutations in the *PNPLA2*-gene leading to a malfunctioning protein (41). Besides deletions and duplication mutations, also single-nucleotide transversions have been identified (36). In many cases these mutations lead to an early terminated translation due to premature stop codons caused by frameshifts or nonsense mutations (36). A considerable proportion of mutations are located at the C-terminal region of the patatin domain (36). The resulting protein is truncated, lagging the hydrophobic C-terminus, and therefore fails to bind LDs properly (32). More recent studies also reported missense mutations in the patatin domain leading to insufficient enzyme activity with proper LD binding (42). Furthermore, NLSDM patients were characterized exhibiting truncated ATGL proteins that lost amino acid residues of the patatin domain (43). It can be assumed that hydrolytic capacities of the truncated protein are completely eliminated. Recently, Pasanisi and colleagues could identify a NLSDM patient with a completely deficient ATGL protein, predicted to consist of only 14 amino acid residues (41).

Since there are numerous mutations causing the disorder with diversified severity, the onset of NLSDM can vary drastically. Late onsets at an age of over 60 years are described, as well as onsets during early youth, resulting in a median age of 30 years (44). In all cases TGs accumulate in many tissues and organs, especially in those of cardiac- and skeletal muscle (36). By mechanisms which are yet unknown, the accumulation of lipids is connected to skeletal muscle weakness and myopathy. Decreasing muscle strength limits motor skills and restricts mobility. Considering cardiac TG aggregation, the affliction is more serious due to manifestations of severe cardiomyopathy (36), in some cases referred to as cardiomyovasculopathy (TGCV) (45). Pronounced malfunction can become a life-threatening event requiring heart transplantation. Interestingly, NLSDM patients are not obese. About 30% develop diabetes and about 50% liver disorders such as hepatomegaly or liver steatosis (36) (44). In contrast to NLSDI, ichthyosis never occurs in NLSDM patients (44). Neurological disorders usually only appear in NLSDI, but in one case of NLSDM cognitive impairment was reported (46), suggesting brain involvement can’t be ruled out in NLSDM patients.

1.2 Skeletal muscle

Body movements and visceral actions requiring any form of motility are facilitated by the muscular system. The contractile tissues of this organ are classified into three types, according to their structure, function and mode of action. Smooth muscle tissue is responsible for the stabilization and motile actions of visceral organs like the gastrointestinal tract, blood vessels and respiratory tract. Smooth muscles are innervated by the autonomic nervous system and therefore involuntary muscles. A similar statement can be made for cardiac muscles. Cells of this tissue regulate their contractility autonomously by a region called the sinu-atrial node. Cardiac muscles belong to the striated muscles and only appear in the heart. The third major muscle tissue type is the skeletal muscle (reviewed in (47)). In contrast to cardiac muscle, skeletal muscle is a striated muscle voluntarily controlled. Furthermore, skeletal muscle is distributed across the whole body. It is a dynamic organ with essential functions in physical health and mobility.

1.2.1 Skeletal muscle structure

Skeletal muscle provides the power necessary for the body to move by a contracting mechanism which shortens the muscle length upon energy consumption. To translate the contraction force into a movement, the muscles are attached to bones of the skeleton via collagenous fibers known as tendons. The entity responsible for muscle contraction is the myofiber, which corresponds to the muscle cell (myocyte). These specialized cells are of an elongated shape and contain multiple nuclei. Grouped myofibers enveloped by a connective tissue sheet (perimysium) are called fascicles. Fascicles are further clustered together to constitute the muscle, which is also coated by a connective tissue sheet (epimysium). Muscles contain a pronounced blood vessel network to cope with the high nutrition and oxygen demand. Furthermore, the myofibers within the fascicles are innervated by nerves of the somatic nervous system at specialized synapses called neuromuscular end-plate. This allows muscle groups to perform coordinated contractions upon signals from the brain.

The plasma membrane of myofibers, also known as sarcolemma, is surrounded by a basal membrane which is associated with a connective tissue sheet (endomysium). Protein complexes within myofibers anchored to the cell wall perform the contraction reaction. These complexes known as myofibrils, consist of sarcomere subunits connected end-to-end. Sarcomeres mainly consist of actin and myosin protein members that perform the shortening reaction by an ATP

driven mechanism. During this process, actin and myosin proteins slide along each other, shortening the length of the sarcomere and subsequently of the muscle. Alpha-actinin is an important protein stabilizing actin in the sarcomeric complex.

Myofibers mainly derive from a muscle stem cell population called satellite cells (see 1.2.2) (reviewed in (48)). These cells rest in a quiescent state between the sarcolemma and the basal membrane (48). During embryogenesis, post-natal muscle growth and upon repair responses, these cells get activated, start to differentiate and fuse to multinucleated muscle fibers (49). Besides satellite cells, muscle side population (SP) cells, $PW1^{+}$ interstitial cells, mesangioblasts and pericytes were also shown to possess myogenic potential (49). However, the contribution of these cells to in vivo muscle development is still under investigation.

Myofibers are classified into different types according to diverse characteristics. Depending on their main source of energy, myofibers preferably using fatty acids, are known as oxidative fibers due to aerobic β-oxidation. Slow twitch or type-I myofibers are other common terms. These fibers are more resistant to fatigue and therefore mainly occur in muscles which require high endurance capabilities. Those muscle fibers depending heavily on breakdown of carbohydrates are classified as glycolytic fibers. They are also referred to as type-II or fast twitching fibers. In contrast to type-I, the anaerobic burst-like mode of action results in rapid fatigue of type-II fibers. Because of further differences and intermediate variants, sub classifications are sometimes applied. Since muscles of different locations are confronted with different challenges, they have a diverse fiber type composition which can be altered to a certain degree by resistance training.

It should also be mentioned that skeletal muscle possesses further critical functions in body homeostasis. In cold conditions, fast muscle contractions known as shivering provide heat to maintain a physiological body temperature. In times of malnutrition and fasting, crucial metabolites like amino acids and carbohydrates can be retrieved from skeletal muscle stores to supply the organism (50).

1.2.2 Satellite cells are muscular stem cells

Skeletal muscle development and regeneration are based on a specific cell population with stem cell features (reviewed in (49)). According to their location between sarcolemma and basal membrane, they were named satellite cells (51). Satellite cells have stem cell characteristics due to their capability of self-renewal, which allows them to replenish the cell pool of their niche (49).

This ensures multiple rounds of skeletal muscle regeneration where the demand for satellite cells, which reconstitute injured muscles, is high (49).

Under unstimulated conditions satellite cells remain in a quiescent (G0) resting state expressing the paired box transcription factor Pax7 (52). Pax 7 is thought to be a key component in regulating the myogenic program, together with other myogenic regulatory factors (MRFs). It is assumed that Pax7 maintains the quiescent state by impeding the action of MRFs which promote differentiation by a reciprocal inhibition mechanism (53). Further studies have showed that Pax7 is the canonical marker for satellite cells (52). The labeling of surface proteins laminin and M-cadherin by immunofluorescent techniques, allows fluorescence microscopy of satellite cells located to myofibers (54).

Upon receiving signals, such as released mitogens from damaged muscles, satellite cells are activated, enter the cell cycle and start to proliferate (55). An early TF upregulated during the myogenic differentiation is myogenic factor 5 (Myf5) (56). Interestingly, Myf5 is already present in 90% of quiescent satellite cells to a certain degree (57). Therefore Myf5 appearance seems to mark myogenic commitment, which is further substantiated by the accompanied expression of MyoD (58). Together, these TFs are characteristic orchestrators of activated satellite cells, which proliferate and subsequently turn into myoblasts (see Figure 2) (49). Pax7 on the contrary, gets downregulated as the differentiation progresses (53). After limited rounds of proliferation, the terminal differentiation of myoblasts towards myotubes goes along with the up regulation of TFs myogenin (MyoG) and Mrf4, (59). During this late phase, myoblasts fuse to each other or to existing myotubes, leading to the formation of polynucleated myotubes (49). In vivo they are referred to as myofibers.

Satellite cells in cell culture were shown to spontaneously differentiate into multiple mesenchymal lineages (49). Besides the differentiation towards myocytes, they turned into adipocytes and osteocytes (60). Whether adipogenic and osteogenic differentiation of satellite cells also occurs in vivo can be doubted, since recent studies have found a different cell type likely to account for white adipocyte formation. Due to their fibrogenic and adipogenic potential, these cells were named fibro/adipogenic progenitors (FAP) (61; 62). Whenever the integrity of the environment these cells reside in is disturbed, FAPs differentiate into adipocytes (see 1.2.3). Further studies could finally exclude that white adipocytes found in skeletal muscle were derived from satellite cells. Lineage tracing has shown that these adipocytes had never expressed the transcription factor Pax3, which invariably occurs during satellite cell development (63).

To investigate myogenic differentiation in cell culture, C2C12 cells constitute an appropriate model. This adherent mouse myoblast cell line is derived from myogenic cells isolated by Yaffe and Saxel (64). The subclone, which is now commercially available was produced by Blau et al. (65) and has the capability to differentiate into myotubes, which express muscle specific proteins. Concerning myogenic lineage, C2C12 cells exhibit a more committed myoblast state than satellite cells, accompanied by the expression of associated TFs. Recent studies reported that C2C12 cells express the transcriptional co-activator PGC-1α, which promotes the myogenic differentiation towards type-I myofibers (66). This led to the assumption that differentiated C2C12 myotubes show muscle fiber type-I characteristics.

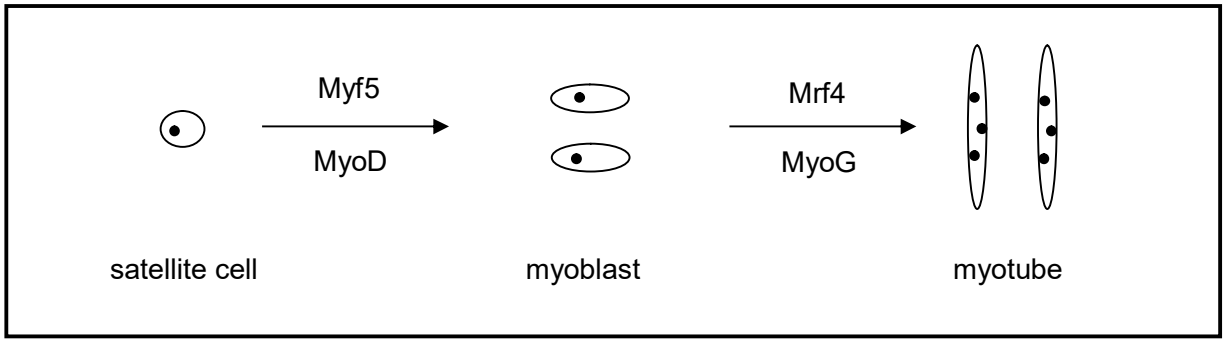

Figure 2: Myogenic differentiation states of satellite cells. Activated satellite cells up regulate Myf5 and MyoD and turn into myogenic committed myoblasts. Myoblasts express Mrf4 and MyoG while fusing to each other or to existing myotubes. As a result polynucleated myotubes, also known as myofibers, appear. Abbreviations: Myf5, myogenic factor 5; MyoD, myogenic differentiation 1; Mrf4, myogenic regulatory factor 4; MyoG, myogenin

1.2.3 Physiological and non-physiological skeletal muscle dysfunctions

Skeletal muscle diseases are events that disturb physiological muscle integrity and function to various degrees. The symptoms can range from weak cramps that barely affect everyday life to severe muscle degeneration with life-threatening respiratory disorders causing premature death. Whenever a disease impairs the function of muscle fibers resulting in muscle weakness, the disorder is referred to as myopathy. Besides reduced muscle strength, symptoms of myopathy comprise stiffness, cramps and tetany.

Most myopathies are classified based on the different factors that cause them. Metabolic myopathies are the result of abnormalities in the lipid, carbohydrate, nucleotide or mitochondrial metabolism of the muscle (reviewed in (67)). In cases of a misguided immune defense system, skeletal muscle can become the focus of the immune response which then causes chronic muscle inflammation. These inflammatory myopathies are therefore the result of a systemic autoimmune disease (reviewed in (68)). Whenever drug intake or the uptake of a toxin causes morbid conditions in skeletal muscle, they are referred to as toxic myopathies (reviewed in (69)). Pathological mechanisms and symptoms of toxic myopathies are manifold, depending on the incorporated substance. Many myopathies caused by genetic mutations are summarized under the term muscular dystrophy. Muscular dystrophies are characterized by a progressive degeneration of skeletal muscle associated with histological changes and alterations in muscle fiber dimensions, mostly induced by mutations in structural muscle proteins (reviewed in (70)). In the case of duchenne muscular dystrophie (DMD), a more prevalent dystrophy form, muscle integrity is disturbed by mutations in the gene of the structural protein dystrophin, resulting in quickly progressing muscular weakness (reviewed in (71)). Further myopathy variants, some of minor prevalence, are described in the literature.

Skeletal muscle weakness is not predominantly associated with severe muscle diseases. In fact, the age-related muscle loss accompanied by locomotive disabilities; the major characteristics of sarcopenia, is a very common syndrome (reviewed in (72)). Sarcopenia is characterized by muscle atrophy leading to muscle weakness (72). The condition is primarily a result of physical inactivity and malnutrition, often triggered by further diseases and therefore mainly associated with the elderly (72). During the progression of the disease, the muscle tissue gets substituted by fat tissue which constitutes the intramuscular adipose tissue (IMAT) (73). IMAT is a common sign of muscle degeneration, characterized by the formation of white adipocytes within the interstitium of skeletal muscle (reviewed in (74)).

A key feature of the muscle system is the capacity to regenerate damaged areas by the fusion of muscle stem cells (see 1.2.2). In situations where the regeneration process is corrupted by diseases, ectopic fat tissue arises within the muscles forming IMAT (reviewed in (73)). The exact mechanism behind the fatty infiltration is still under investigation, however, the main cell type differentiating into white adipocytes was found recently. These PDGFRα expressing FAPs seem to be a crucial cell population maintaining a healthy muscle status under physiological conditions (61; 62; 63). Whenever a disease adversely changes the interstitial milieu of the muscle, FAPs get stimulated to reprogram their fate and differentiate towards white adipocytes. The emergent

muscular fat is far from being considered inert. It is rather recognized as an active hormone-secreting entity which influences the local muscle milieu, impinging its myogenic capacity.

To study muscular damage and regeneration mechanisms, intramuscular adipocyte formation is artificially induced by the application of chemical substances into the skeletal muscle. The injected chemicals harm the tissue and trigger a regeneration response. Depending on the substance employed, adipocytes are formed in a certain amount after the healing process is completed. These injections can be performed in genetically modified mice, where the magnitude of fatty infiltration can be determined by the size of the ectopic fat area. The information assessed allows conclusions regarding the genetic background and its influence on degenerative processes to be drawn. Cardiotoxin and notexin are frequently used to induce muscle damage yielding only minor adipocyte amounts. More promising is the recently established glycerol injection model (75). The glycerol which is hereby injected, induces myofiber necrosis by disrupting the cell membrane (75). In the following 3 weeks regeneration processes reconstitute the original muscle structure, accompanied by white adipocyte development toward the end (75). Three month-old mice were reported to develop a fat area of up to 5% within the skeletal muscle, when the glycerol approach is applied (75).

1.2.4 ATGL in skeletal muscle

As one would expect, ATGL is exclusively expressed in type-I myofibers (76). These oxidative cells depend heavily on the liberation of FFAs by ATGL, since fatty acids are the main metabolites fueling mitochondrial beta-oxidation. As already mentioned, aerobic energy production is the hallmark of type-I fibers. NLSDM patients suffering from ATGL deficiency develop a noticeable metabolic myopathy with progressing muscle weakness, especially in the limbs (36; 77). In severe cases, decreased muscle strength disables patients to raise arms over the horizontal position (42). The characteristic lipid accumulation found in most tissues of the body, is very pronounced in myocytes of NLSDM patients (78).

The mechanism behind the muscle weakness in individuals suffering from NLSDM is still under investigation. A recent study linked disturbances in lipid signaling upon ATGL decrement with signs of muscular degeneration (79). Aquilano and colleagues were able to show that skeletal muscles of 80-week-old mice display characteristics of muscle damage which goes along with decreased ATGL expression (79). They found reduced antioxidative capacity due to ATGL deficiency to be responsible for muscle degeneration (79).

Unpublished data by Matthijs Hesselink's[1] group has shown intriguing effects of ATGL deficiency on human satellite cells. They have been able to show that satellite cells isolated from NLSDM patients via muscle biopsy possess severely impaired myogenic differentiation properties. Fluorescence microscopy revealed that these cells remained in a roundish shape upon myogenic induction, whereas control cells formed characteristic myotubes. Since satellite cells are described as the cell population used as a key source during the development of regenerative muscle tissue, these differentiation disturbances could be the reason for muscle atrophy in patients suffering from NLSDM.

[1] Matthijs Hesselink, Diabetes and Metabolism Research Group, Maastricht University, Netherlands

2 Aim of the study

The aim of the study was to investigate the impact of ATGL deficiency on skeletal muscle integrity. Patients suffering from mutations in the *ATGL*-gene develop myopathies with pronounced muscle atrophy, leading to muscular weakness (36). To elucidate whether the differentiation of myocytes is impaired upon reduced ATGL activity, we performed differentiation studies in a mouse myoblast cell line (C2C12) expressing or not expressing ATGL. Furthermore, we aimed to establish a protocol to isolate primary muscle stem cells from mice and analyze their differentiation potential. Since aged humans show symptoms of muscular dysfunction, we investigated whether this also translates into old mice which would make them a proper model for muscular disorders. Finally, we attempted to implement a muscle regeneration model in which intramuscular glycerol injection results in adipocyte formation to investigate whether ATGL affects muscle cell regeneration.

3 Materials

3.1 Media

Dulbecco's Modified Eagle Medium high glucose

(DMEM high glucose, Gibco by life technoligies, Carlsbad, USA)

4.5 g/l glucose
100 U/ml penicillin/ 100 µg/ml streptomycin
0.5 µg/ml puromycin

For cell growth: 20% FCS

For myogenic media: 2% FCS

For adipogenic induction media: 10% FCS, 10 µg/ml insulin, 1 µM dexamethasone, 2 µM rosiglitazone, 0.5 mM IBMX

For adipogenic maintenance media: 10% FCS, 10 µg/ml insulin, 2 µM rosiglitazone

Dulbecco's Modified Eagle Medium: Nutrient Mixture F-12 GlutaMAX™

(DMEM/F-12 + GlutaMAX™, Gibco by life technologies, Carlsbad, USA)

100 U/ml penicillin/ 100 µg/ml streptomycin
100 µg/ml primocine

For cell growth: 20% FCS

For myogenic media: 2% FCS

For adipogenic media: 10% FCS, 10 µg/ml insulin, 1 µM dexamethasone, 2 µM rosiglitazone, 0.5 mM IBMX

3.2 Buffers and Solutions

1x PBS (pH 7.3)

140 mM NaCl
2.7 mM KCl
10 mM Na 2 HPO 4
1.8 mM KH 2 PO 4

PBT

0.1% Triton X-100 in 1x PBS

1000x protease inhibitor (Pi)

20 mg leupeptin
2 mg antipain
1 mg pepstain
1 ml DMSO
sterile filtered

1x TAE buffer (pH 7.2)

40 mM Tris/HCl
50 mM EDTA
7 % glacial acetic acid

1x TST (pH 7.4)

50 mM Tris/HCl
0.15 M NaCl
0.1% Tween 20

4x lower buffer (pH 8.8)

0.5 M Tris
0.4% SDS stored at 4°C

4x upper buffer (pH 6.8)

0.5 M Tris stored at 4°C

4x SDS loading buffer (pH 6.8)

0.2 M Tris
10% β-mercaptoethanol
8% SDS
40% glycerin
bromophenol blue (tip of a spatula)

Coomassie staining solution

50% ethanol
7.5% from 80% acetic acid
0.25% Coomassie brilliant blue R250

Coomassie destaining solution

10% from 80% acetic acid
30% methanol

Agarose 1%

300 ml ddH 2 O
3g agarose
6ml 50x TAE
20µl ethidium bromide

CAPS transfer buffer (pH11)

10 mM CAPS
10% methanol

DEPC water

1ml diethylpyrocarbonate in 1L H_2O

RNA loading dye

48% formamide
9% 10 x MOPS
6% formaldehyde
31% DEPC H2O
5% sterile glycerol
1% ethidium bromide (10 mg/ml)

10x SDS-PAGE running buffer

200 mM Tris
1.6 M glycine
0.83 % SDS

3.3 Cell lines and primary cells

All cultured cells were grown in 175 cm² cell culture flasks containing denoted Media. The cultivation was carried out in incubators at 7% CO_2, 37°C and 95% air humidity. To avoid contaminations and maintain sterility, for all treatments a “laminar flow” was used.

C2C12 cells with a lentiviral ATGL knockdown

C2C12 cells are a adherent growing myoblast cell line derived from mouse muscles. The cells used in the experiments were obtained from a previous student of Dr. Martina Schweiger who generated cells with a knockdown of the ATGL gene (*PNPLA2*) by using a lentiviral system to introduce small interfering RNA (siRNA). Four different cell clones containing different siRNA sequences were used for the experiments. Two clones were transfected with scrambled siRNA sequences and therefore used as controls. The other two clones were transfected with two different siRNA sequences designed to specifically silence the *ATGL*-gene by RNA interference (RNAi). For cultivation, DMEM high glucose media with 20% FCS, 1% penicillin/streptomycin mix and 0.5 µg/ml puromycin was used.

Primary mouse satellite cells

The primary muscle stem cells isolated from mouse gastrocnemius and tibialis anterior muscles were cultured in DMEM/F-12 + GlutaMAX™ media containing 20% FCS, 1% penicillin/streptomycin mix and 100 µg/ml primocine.

3.4 Mice

C57BL/6J mice with a homozygous ATGL-deficient Atgl (-/-) genotype were generated as described by Haemmerle et al. (35). The mice were kept at a 14-hour light 10-hour dark cycle in a pathogen free animal facility with free access to a standard chow diet (4.5% w/w fat).

3.5 Primers

Table 1: Primers for qRT-PCR. The Primers used for quantitative real-time Polymerase chain reaction (qRT-PCR) are listed with their nucleotide sequence.

Primer	Sequence
Pax7	Fwd: 5- GACGACGAGGAAGGAGACAA-3‘ Rev: 5- ACATCTGAGCCCTCATCCAG-3‘
MHC2B	Fwd: 5'- AGTCCCAGGTCAACAAGCTG -3' Rev: 5'- TTTCTCCTGTCACCTCTCAACA -3'
MyoD	Fwd: 5'- ACTTTCTGGAGCCCTCCTGGCA -3' Rev: 5'- TTTGTTGCACTACACAGCATG -3'
FABP4/aP2	Fwd: 5'-AAGGTGAAGAGCATCATAACCCT-3' Rev: 5'-TCACGCCTTTCATAACACATTCC-3'
SCD1	Fwd: 5'-CCTGCGGATCTTCCTTATCATT-3' Rev: 5'-GTGGGCGCGGTGATCTC-3'
PPARg2	Fwd: 5'-CCAGAGCATGGTGCCTTCGCT-3' Rev: 5'-CAGCAACCATTGGGTCAG-3'
Col1a2	Fwd: 5' AAGGGTGCTACTGGACTCCC 3' Rev: 5' TTGTTACCGGATTCTCCTTTGG3'
ATGL	Fwd: 5’- GAGACCAAGTGGAACATC -3’ Rev: 5’- GTAGATGTGAGTGGCGTT -3’

Atrogin	Fwd: 5'- CTTTCAACAGACTGGACTTCTCGA -3 Rev: 5'- CAGCTCCAACAGCCTTACTACGT -3
Murf-1	Fwd: 5'- AGTGTCCATGTCTGGAGGTCGTTT -3 Rev: 5'- ACTGGAGCACTCCTGCTTGTAGAT -3

3.6 Antibodies

Table 2: Antibodies for western blot analysis and fluorescence microscopy. Primary and secondary antibodies are listed.

Primary antibody	Secondary antibody
Anti-ATGL 1:1000, 5% milk in 1x TST	Anti-rabbit HRP conjugated goat IgG (Vector Laboratories), 1:10000, 5 % milk in 1x TST
Anti-LC3B, 1:1000; 5% BSA in 1x TST	Anti-rabbit HRP conjugated goat IgG (Vector Laboratories), 1:10000, 5 % milk in 1x TST
Anti-GAPDH (Cell signaling), 1:10000, 5% milk in 1x TST	Anti-rabbit HRP conjugated goat IgG (Vector Laboratories), 1:10000, 5 % milk in 1x TST
Anti-Pax7 (Sigma), 1:2000, 1% BSA in PBT	Anti-mouse Rhodamine labeled IgG (GE healthcare) 1:1000, 1% BSA in PBT
Anti-α-Actinin (Cell singaling), 1:25, 1% BSA in PBT	Anti-rabbit DyLight® 488 labeled IgG (Thermo Fisher), 1:1000, 1% BSA in PBT

3.7 Standards

The Precision Plus Protein™ All blue Standards (Bio-Rad Laboratories Inc., Hercules, USA) was used for western blot analysis.

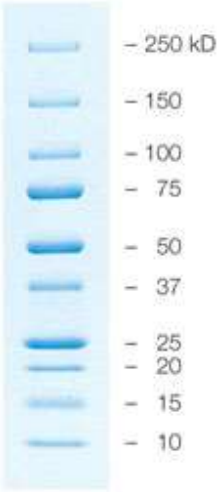

Figure 3: Bio-Rad Precision Plus Protein™ All blue Standards.

3.8 Kits

- **Bio-Rad Laboratories, Inc (Hercules, USA)**

- Bio-Rad Protein Assay Dye Reagent Concentrate (Bradford assay)

- **Thermo Fisher Scientific Inc. (Waltham, USA)**

- Pierce™ ECL Western Blotting Substrate kit

- Infinity™ Triglycerides Liquid Stable Reagent

- Pierce™ BCA Protein Assay Kit

- High-Capacity cDNA Reverse Transcription Kit

- Maxima SYBR Green/ROX qPCR Master Mix

4 Methods

4.1 Cell culture

4.1.1 Cultivation and harvesting of C2C12 cells

Cultivation of C2C12 cells

Cells were grown in 175 cm² culture Flasks containing DMEM high glucose media (+ 20% FCS, + 100 µg/ml penicillin and 100 µg/ml streptomycin, + 0.5 µg/ml puromycin) till they reached a confluence of about 90%. Then, the cells where washed with 1x PBS, detached using 0.05% Trypsin-EDTA solution (Invitrogen – Life Technologies, Carlsbad, USA) and centrifuged for 3 min at 1200 g after some media was added. The cell pellet was resuspended in media and the cells were counted using a Neubauer cell counting chamber (Brand GmbH & Co. KG, Wertheim, Germany). Cell suspension was seeded in 6-well plates at a concentration of 70 000 cells per well. When cells achieved confluence, media was shifted towards myogenic and adipogenic differentiation media. Throughout cultivation, media was changed every other day. Cells for fluorescence microscopy were seeded in x-well chambers.

Harvesting of C2C12 cells

Cells where washed two times with 1x PBS before 200 µl ice-cold PBS + Pi was administered to each well. The cells where detached with a cell-scraper, transferred into a 1.5 ml tube and centrifuged for 10 min at 800 g. After the supernatant was removed, the cell pellet was stored at -20°C.

4.1.2 Cultivation and harvesting of satellite cells

Cultivation of satellite cells

The cultivation procedure of satellite cells equates to the routine denoted for C2C12 cells (see 4.1.1), except for the applied media. For cell growth DMEM/F-12 + GlutaMAX™ (+ 20% FCS, +

100 µg/ml penicillin and 100 µg/ml streptomycin, 100µg/ml primocine) media was used. Further, satellite cells were grown on gelatin coated flasks and plates. The coating was done by incubating cell culture devices for 1 hour with 0.2% Gelatin solution Type B (Sigma-Aldrich, St. Louis, USA) in a laminar flow hood. Afterwards, the solution was removed and the devices air dried in the hood. Coated devices were stored at 4°C.

Harvesting of satellite cells

The cells were washed with 1x PBS two times before 1 ml of TRIzol® (Thermo Fisher Scientific Inc, Waltham, USA) was added to each well. After 2 minutes of incubation, the suspension was transferred into a 1.5 ml tube and stored at -20°C.

4.2 Determination of gene expression on mRNA level

4.2.1 RNA isolation of C2C12 cells

To isolate RNA from C2C12 cells, 1 ml TRIzol® (Thermo Fisher Scientific Inc, Waltham, USA) was added to the cell pellet. After using a pipette to dissolve the cells, 100 µl bromchloropropan was administered and the suspension was mixed vigorously, followed by 10 minutes of incubation at room temperature. Centrifugation at 12000 g for 15 min at 4°C was applied to separate the phases. The upper phase was collected in a 1.5 ml tube and mixed with 500 µl isopropanol, followed by a second 10 minute incubation at room temperature. After a 10 minute centrifugation at 12000 g and 4°C the supernatant was discarded and the pellet washed with 600 µl 75% Ethanol in DEPC water. The pellet was dried at room temperature and solved in 30 µl DEPC water.

The RNA concentration was determined by measuring 2 µl RNA solution with the NanoDrop Spectrophotometer (Thermo Fisher Scientific Inc., Waltham, USA). The samples were diluted to a concentration of 200 ng/µl. Five µl solution were taken, mixed with 1 µl RNA loading dye and run on a 1.5% Agarosegel. The run was performed for 15 minutes at 80 Volt to compare concentrations and to check for RNA degradation.

4.2.2 RNA isolation of satellite cells

The isolation was performed as denoted for C2C12 cells (see 4.2.1). Since the cells were already dissolved in TRIzol, the isolation was initiated by the addition of bromchloropropan.

4.2.3 RNA isolation of tissue samples

RNA was isolated from one spatula tip of tissue powder. The frozen tissue was powderized on dry ice using a pistil which was frequently cooled by liquid nitrogen. After adding 1 ml TRIzol to the tissue powder in a 2 ml tube, a T 10 basic ULTRA-TURRAX (IKA, Staufen, Germany) was used for 10 seconds on level 3 to homogenize the sample. The following steps were performed as specified for the isolation from C2C12 cells (see 4.2.1).

4.2.4 cDNA synthesis by reverse transcription

The first step in the transcription of mRNA into cDNA was the ablation of DNA by DNase digestion. Therefore 5 µl from 200 ng/µl RNA solution was mixed with 5 µl DNase mastermix containing 1 µl DNase enzyme (1U/µl), 1 µl 10x buffer and 3 µl DEPC water. After 15 minutes of incubation at 25°C 1 µl EDTA solution was added and the samples were heated at 65°C for 10 minutes. Samples were kept on ice between all experimental steps.

For the reverse transcription step 10 µl of the DNase digested sample was mixed with 10 µl reverse transcription mastermix containing 2 µl 10x reverse transcriptase buffer, 0.8 µl 25x dNTP (100 mM), 2 µl 20x random primer, 3.2 µl DEPC water, 1 µl RNase inhibitor (4 U/µl), 1 µl reverse transcriptase enzyme. This was done in PCR-strips which were then used to perform a PCR in the Thermocylcer (Bio-Rad Laboratories Inc., Hercules, USA) with the following protocol:

1. Initiation step: 10 min, 25°C
2. Reverse transcription step: 120 min, 37°C
3. Denaturation step: 5 min, 85°C
4. Cooling: hold, 4°C

The cDNA was diluted 1:5 with Nuclease-Free Water.

4.2.5 Quantitative real-time PCR (qRT-PCR)

For the quantitve measurement of gene expression, 4µl cDNA was added to 16 µl qRT-PCR mastermix containing 10 µl Maxima SYBR Green/ROX qPCR Master Mix, 1 µl forward primer (10 pmol), 1µl reverse primer (10 pmol) and 4 µl Nuclease-Free Water. This was done in 96-well PCR Plates (Bio-Rad Laboratories Inc., Hercules, USA) which were sealed and analyzed in a Bio-Rad C1000™ Thermal Cycler with CFX96™ Real-Time System (Bio-Rad Laboratories Inc., Hercules, USA) applying the following protocol:

1. Initial step 1: 2 min, 50°C
2. Initial step 2: 10 min, 95°C
3. Melting: 15 sec, 95°C
4. Annealing & extension: 1 min, 60°C
5. 40x repeat of steps 3 & 4
6. Final extension: 1.5 min, 95°C

4.3 Determination of Lipid content

4.3.1 Lipid isolation of C2C12 cells

The cells were washed three times with 1x PBS before 500 µl ice-cold (-20°C) hexane-isopropanol (3:2) was added to each well of a 6-well plate. After 10 minutes of incubation at room temperature the liquid phase was transferred into a 1.5 ml Tube. These steps were repeated for two times before the collected lipid solution was dried under nitrogen. After washing the lipid remains with 500 µl of chloroform they were again dried under nitrogen. The dried lipids were dissolved in 300 µl 2% Triton X-100 in ddH_2O.

4.3.2 Lipid isolation of tissue samples

Lipids were isolated from two spatula tips of tissue powder. Therefore the frozen tissue was powderized on dry ice using a pistil which was frequently cooled by liquid nitrogen. At first, 200 µl 1x PBS, than 1.5 ml Folch solution (chloroform/methanol 2:1) was added to the tissue powder. The suspension was homogenized with a T 10 basic ULTRA-TURRAX (IKA, Staufen, Germany)

4-times within 30 minutes, followed by 15 minutes of incubation at 21°C and 900 rpm in a Thermomixer (Eppendorf AG, Hamburg, Germany). Centrifugation at 3500 g for 10 minutes yielding a phase separation facilitates to take the lower phase by generating a small hole in the bottom of tube. This was done with a hot needle. 500 µl of the collected lower phase was transferred in a new tube and evaporated under nitrogen. The dried lipids were dissolved by adding 300 µl 2% Triton X-100 in ddH_2O, followed by sonication with a Misonix sonicator (Misonix, Farmingdale, USA) for 10 seconds on Amplitude 1.

4.3.3 Infinity triglyceride assay

To measure TG content, 20 µl of isolated lipid samples or standards were mixed with 150 µl Infinity™ Triglycerides Liquid Stable Reagent (Thermo Fisher Scientific Inc., Waltham, USA) in a 96-well plate and incubated for 10 minutes at 37°C. The readout was performed at 492 nm with a Biotrak II Plate reader (Amersham Biosciences, Cambridge, UK). Glycerol Standard Solution (Sigma-Aldrich, St. Louis, USA) was diluted with 2% Triton X-100 in ddH_2O and used as standard. Double determinations were done for each sample and the standard.

4.4 Measuring Protein level

4.4.1 Protein isolation of tissue samples

Protein was isolated from two spatula tips of tissue powder. Therefore the frozen tissue was powderized on dry ice using a pistil which was frequently cooled by liquid nitrogen. At first 200µl 1x PBS, than 1.5 ml Folch solution (chloroform/methanol 2:1) was added to the tissue powder. The suspension was homogenized with a Ultra-Turrax 4- times within 30 minutes, followed by 15 minutes of incubation at 21°C and 900 rpm in a Thermomixer. Centrifugation at 3500 g for 10 minutes yielding a phase separation allowed to take the protein cake by discarding all liquid phases. The protein cake was dried at 90°C for 1 hour in the Thermomixer. Afterwards, the protein was dissolved in 500µl SDS/NaOH (0.2%/0.1N) for 2 hours at 60°C and 1000 rpm.

4.4.2 Protein isolation of C2C12 cells

The cell pellet was dissolved in 200 µl 1x PBS + Pi on ice and centrifuged for 5 minutes at 4°C and 1000 g. Afterwards, the cells were sonicated with a Misonix sonicator (Misonix, Farmingdale, USA) for 10 seconds on Amplitude 1, followed by a 10 minute centrifugation at 4°C and 1000 g. 200 µl of the supernatant were transferred into a new 1.5 ml tube.

4.4.3 BCA protein assay

The protein concentration in SDS/NaOH (0.2%/0.1N) dissolved samples was determined using the Pierce™ BCA Protein Assay Kit (Thermo Fisher Scientific Inc., Waltham, USA). 20 µl sample or standard were mixed with 200 µl BCA solution in a 96-well plate and incubated for 30 minutes at 37°C. The readout was performed at 562 nm with a Biotrak II Plate reader (Amersham Biosciences, Cambridge, UK). BSA (2 mg/ml) was diluted with SDS/NaOH (0.2%/0.1N) and used as standard. Double determinations were done for each sample and the standard.

4.4.4 Bradford assay

To determine the protein concentration of samples dissolved in 1x PBS +Pi, the Protein Assay Dye Reagent Concentrate (Bio-Rad, Hercules, USA) was used. In a 96-well plate 20 µl sample or standard were mixed with 200 µl Bradford solution and the readout was performed at 620 nm with a Biotrak II Plate reader (Amersham Biosciences, Cambridge, UK). BSA (2 mg/ml) was diluted with 1x PBS + Pi and used as standard. Double determinations were done for each sample and the standard.

4.4.5 SDS-PAGE

To separate the proteins according to their size, a sodium dodecyl sulfate (SDS) - polyacrylamide gel electrophoresis (PAGE) was performed. The gel was constituted by a stacking gel and a separation gel. At first the separation gel was prepared by filling the separation gel solution (see Table 3) between a glas plate and a aluminum silicate plate. These plates were separated by spacers and fixed by clamps. Finally butanol was placed on top to avoid evaporation. After hardening, the stacking gel solution (see Table 3) was added and slots were generated by inserting a comb. The gel was used 30 minutes later.

For the separation in the gel, the samples (see. 4.4.1 and 4.4.2) were diluted according to the concentrations determined in the assays to achieve a protein amount of 50 µg (see 4.4.3 and 4.4.4). 4x SDS loading buffer containing β-mercaptoethanol was added to the protein samples and heated for 10 minutes at 95°C and 300 rpm. After placing the gel in the gel stand, the construct was covered with SDS-PAGE running buffer and the samples were loaded into the slots using a Hamilton syringe. 5 µl of the Precision Plus Protein All Blue Standard (Bio-Rad Laboratories Inc., Hercules, USA) was loaded as standard. The electrophoresis was performed with 20 mA per gel for about 80 minutes, till the running front reached the bottom end.

Table 3: Components of the separating and the stacking gel.

Components	10% separating gel solution (40 ml)	5% stacking gel solution (5 ml)
ddH_2O	16.4 ml	2.95 ml
4x upper buffer	-	1.25 ml
4x lower buffer	10.0 ml	-
30% acryl amide	13.2 ml	0.75 µl
10% SDS	400 µl	50 µl
Tetramethylethylendiamin (TEMED)	36 µl	6.5 µl
10% ammonium persulfate (APS)	108 µl	20 µl
0.5% Bromphenol blue	-	3 µl

4.4.6 Western blot

Blotting and sandwich construction

The gel containing the SDS-PAGE separated proteins was blotted onto a polyvinylidene fluoride membrane (Roti®-PVDF, pore size 0.45 µm; Carl Roth GmbH, Karlsruhe, Germany). Therefore the stacking gel was removed and separating gel was placed on a filter paper, which was put on a sponge. This was done in 1x CAPS transfer buffer. The PVDF membrane was saturated with methanol and placed on the gel. A second filter paper and a second sponge were placed on the PVDF membrane and the construct was transferred into a blot chamber, filled with 1x CAPS transfer buffer. The blotting was performed at 200 mA and 600 Volt for 65 minutes.

Blocking and antibody detection

After the proteins where transferred onto the PVDF membrane, the membrane was blocked with 10% dry milk powder in 1x TST at 4°C overnight. In the following step, the membrane was incubated for 1 hour with the primary antibody at room temperature before it was washed three times with 1x TST for 10 minutes. Then the membrane was incubated with the secondary antibody for 1 hour at room temperature. Afterwards, the membrane was again washed three times with 1x TST for 10 minutes and the antibody was detected with the Pierce™ ECL Western Blotting Substrate kit (Thermo Fisher Scientific Inc., Waltham, USA). The membrane was incubated with the ECL solution for 2 minutes in a dark room before it was placed in a cassette and covered with a photo film. The incubation time in the closed cassette depended on the intensity of the signal. The film was then transferred into a developing solution, washed with water and fixed in fixation solution. To remove all remains of the solutions, the membrane was again washed with water.

Coomassie Blue staining

The membrane was transferred into Coomassie staining solution for five seconds, followed by 15 minutes destaining in Coomassie destaining solution. Thereafter, the membrane was dried under the vent.

4.5 Fluorescence microscopy of C2C12 cells

The cells cultured in 8-well chamber slides were conserved in formaldehyde solution till used for fluorescence microscopy. Therefore the cells were washed 3 times with 1x PBS and incubated with 4% formaldehyde in 1x PBS for 20 minutes at room temperature. Then, the washing steps were repeated and the cells stored in 1xPBS at 4°C.

After the fixation, cells were incubated with 0.1% Triton X-100 in PBS for 10 minutes at room temperature. Then the cells were washed with 0.1% Tween-20 in PBS (PBT) for 10 minutes at room temperature. This was repeated two times, before the cells were blocked with 1% BSA in PBT at 4°C for 1 hour. The primary antibody was diluted in 1% BSA in PBT and added overnight at 4°C. Afterwards, four 10 minutes wash cycles with PBT were carried out, before 1% BSA in PBT was added to block for 15 minutes at room temperature. The fluorescent labeled secondary antibody was diluted in 1% BSA in PBT and added for 1 hour at room temperature. After three 10 minute wash cycles with PBT, the cells were covered with PBS and the fluorescence microscopy was performed using a Leica SP5 confocal microscope with a Leica HCX 63x 1.4 NA objective.

5 Results

5.1 The influence of ATGL on C2C12 myoblast differentiation in cell culture

To investigate whether ATGL has an influence on C2C12 differentiation, we used lentiviral silenced C2C12 myoblasts and applied myogenic and adipogenic differentiation protocols. The cells were analyzed by determining expression levels of marker genes. Furthermore lipid levels were measured to check for TG accumulation due to ATGL ablation. Finally cell morphology during myogenic differentiation was observed by fluorescence microscopy.

5.1.1 Confirmation of the lentiviral ATGL knockdown in C2C12 myoblasts

We obtained different C2C12 clones which were stably infected with different lentiviral siRNA constructs targeting ATGL. To determine the knockdown efficiency of the different siRNA constructs ATGL expression was analyzed by western blot analysis and qRT-PCR. The protein levels (Figure 4 A & B) revealed, that siRNA constructs introduced into clone 774 and clone 777 showed the most powerful result, with a knockdown of over 95% compared to clones 002 and 016 which were infected with scrambled sequences and therefore used as control. Since clones 775, 776 and 511 showed higher ATGL protein levels, they were excluded from further experiments. These were then performed with clones 774 and 777.

Since silencing effects can be altered during different cell phases like differentiation, we surveilled mRNA levels in the chosen clones during 6 days of myogenic differentiation by qRT-PCR analysis (Figure 5). The results showed that ATGL expression in control cells increased over 3-fold during the differentiation. Cells of clone 774 kept a proper ATGL knockdown over the 6 day time period, whereas mRNA level of clone 777 cells rose close to 2-fold when compared to the control on day 1. This implicated that further studies were able to draw a correlation between the ATGL amount and the subsequent changes, given that clone 777 displayed a silencing effect which remained between the ATGL level of the control and the ATGL level of clone 774.

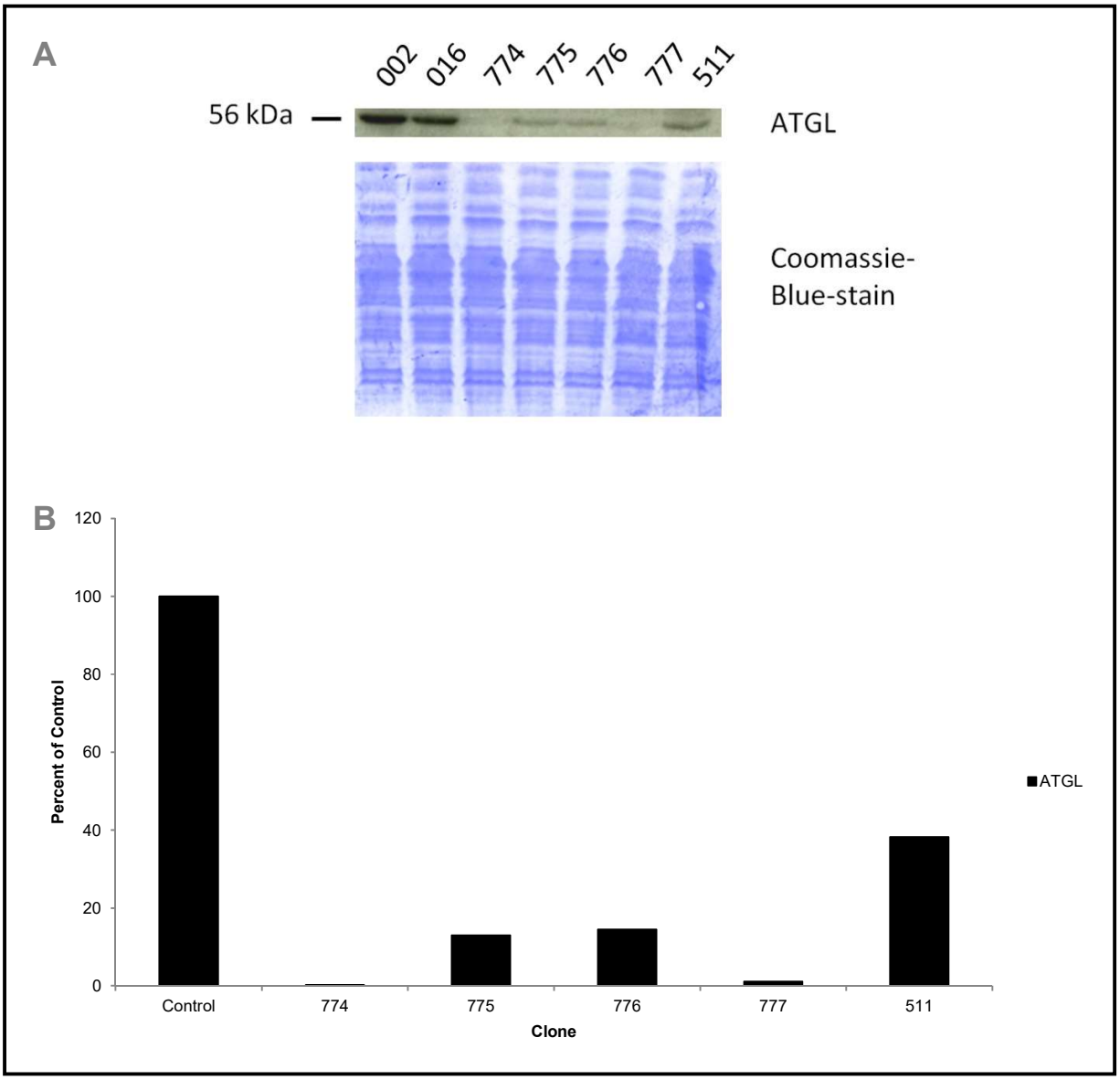

Figure 4: The ATGL protein level of lentiviral silenced C2C12 cells shows a strong knockdown for clones 774 and 777. The western blot analysis **(A)** was performed of undifferentiated C2C12 cells which were infected with lentivirus encoding for different siRNAs. Clones 002 and 016 transfected with different scrambled sequences were used as Control. Clones 774, 775, 776, 777 and 511 were transfected with different siRNA sequences which specifically silence ATGL gene expression. 50 µg protein lysate was used for western blot analysis. Protein transfer was confirmed by Coomassie Blue staining of the membrane. Scanning of the blots and image analysis using Quantity One® 1-D analysis software revealed a knockdown of over 95% for clones 774 and 777 **(B)**.

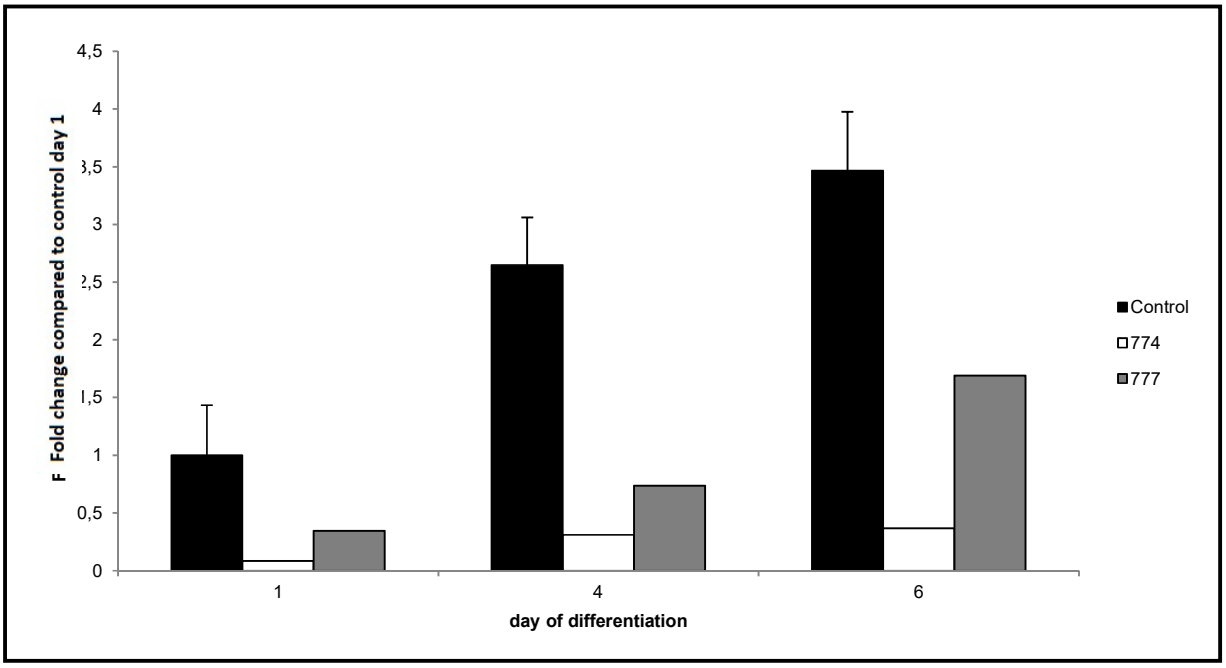

Figure 5: ATGL gene expression in clone 774, clone 777 and the control during 6 days of myogenic differentiation. After ATGL silenced C2C12 cells were grown till density, the DMEM high glucose media containing 20% FCS was replaced by a 2% FCS media to induce myogenic differentiaton. Cells were harvested at indicated time points and analyzed for ATGL mRNA expression by qRT-PCR (normalized to 1).

5.1.2 Myogenic differentiation properties of ATGL silenced C2C12 myoblasts

ATGL silenced C2C12 myoblasts were seeded in 6-well plates containing DMEM high glucose media with 20% FCS to study myogenic differentiation properties. After reaching confluence, the media was changed to DMEM high glucose media containing 2% FCS (myogenic induction media) to induce myogenic differentiation. The cells were harvested at days 0,2,4,6 and 8 of differentiation. Since the clones 774 and 777 behaved identical during myogenic differentiation studies the results were combined and referred to as “ATGL knockdown”.

<u>mRNA levels of differentiation markers</u>

One approach to determine the myogenic differentiation abilities of ATGL silenced C2C12 cells was to analyze the mRNA amount of specific genes which can be considered as markers for

myogenic or adipogenic differentiation. Primers for MHC2B, MyoD and Pax7 were used for qRT-PCR analysis to confirm myogenic differentiation.

As shown in Figure 6, mRNA levels of structural protein MHC2B and the myogenic transcription factor MyoD increased during differentiation, evidencing a successful myogenic differentiation for wild type and knockdown cells. MHC2B, a structural protein in the sarcomeres, increased about 3500-fold in silenced cells compared to the control on day 0 (Figure 6 A). This increase is about twice as high as the increase seen in the control, indicating a higher potential towards myogenic differentiation in ATGL knockdown cells. With a 3.5- fold increase, MyoD levels in ATGL silenced clones rise higher than the control clones which displayed a 2.5-fold gain (Figure 6 B). Despite a short increase, Pax7 gene expression has reached its basal level in C2C12 myoblasts, since the levels did not drop further than the initial value (Figure 6 C).

To clarify whether adipocytes were formed during the myogenic differentiation, aP2/FABP4 and PPARγ2 mRNA levels were determined. The results show that aP2/FABP4 levels did not change in control cells or in ATGL knockdown cells (Figure 7), leading to the conclusion that no adipocytes were formed. PPARγ2 mRNA was below the detection limit, confirming the assumption.

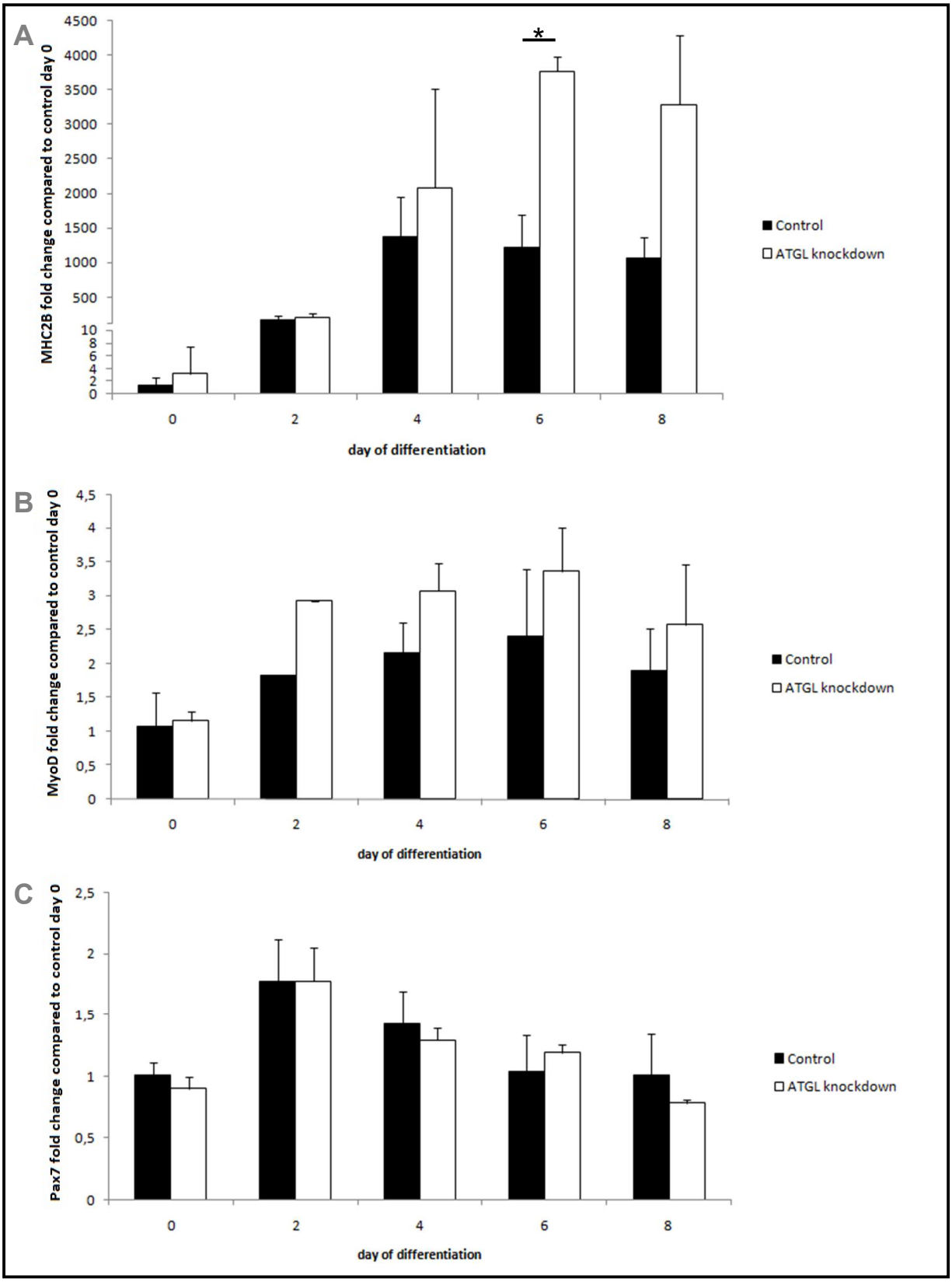

Figure 6: Expression levels of myogenic marker genes MHC2B, MyoD and Pax7 during 8 days of myogenic differentiation. After the C2C12 cells were grown to confluence, the DMEM high glucose media containing 20% FCS

was replaced by a 2% FCS media to induce myogenic differentiation. At indicated time points the cells were harvested and the mRNA level was determined (normalized to 1) using Primers for MHC2B **(A)**, MyoD **(B)** and Pax7 **(C)** genes in qRT-PCR analysis. Error bars represent standard error of the mean, n=2. *$p < 0.05$.

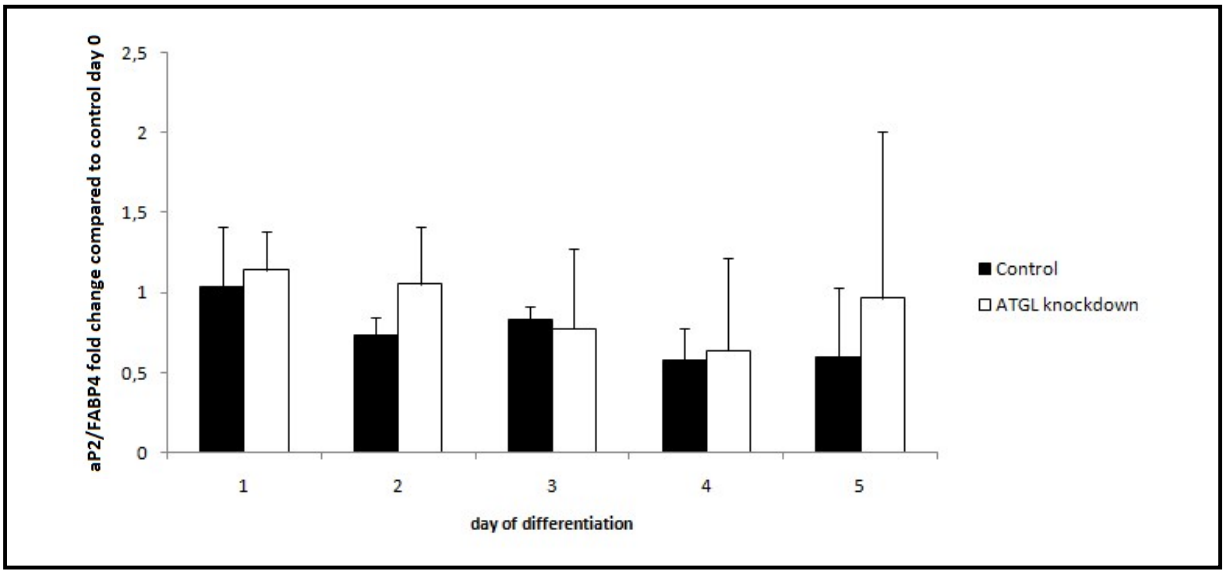

Figure 7: Gene expression of adipogenic marker aP2/FABP4 during 8 days of myogenic differentiation. After the C2C12 cells were grown to confluence, the DMEM high glucose media containing 20% FCS was replaced by a 2% FCS media to induce myogenic differentiation. At indicated time points the cells were harvested and the mRNA level was determined (normalized to 1) using Primers for aP2/FABP4 gene in qRT-PCR analysis. Error bars represent standard error of the mean, n=2.

TG levels of myogenic differentiated cells

To check whether ATGL knockdown in C2C12 cells leads to lipid accumulation during differentiation, like reported for ATGL knockout mouse tissue (35), TG content was measured. ATGL knockdown was associated with a 3-fold increase in cellular TGs levels as compared to control cells (Figure 8).

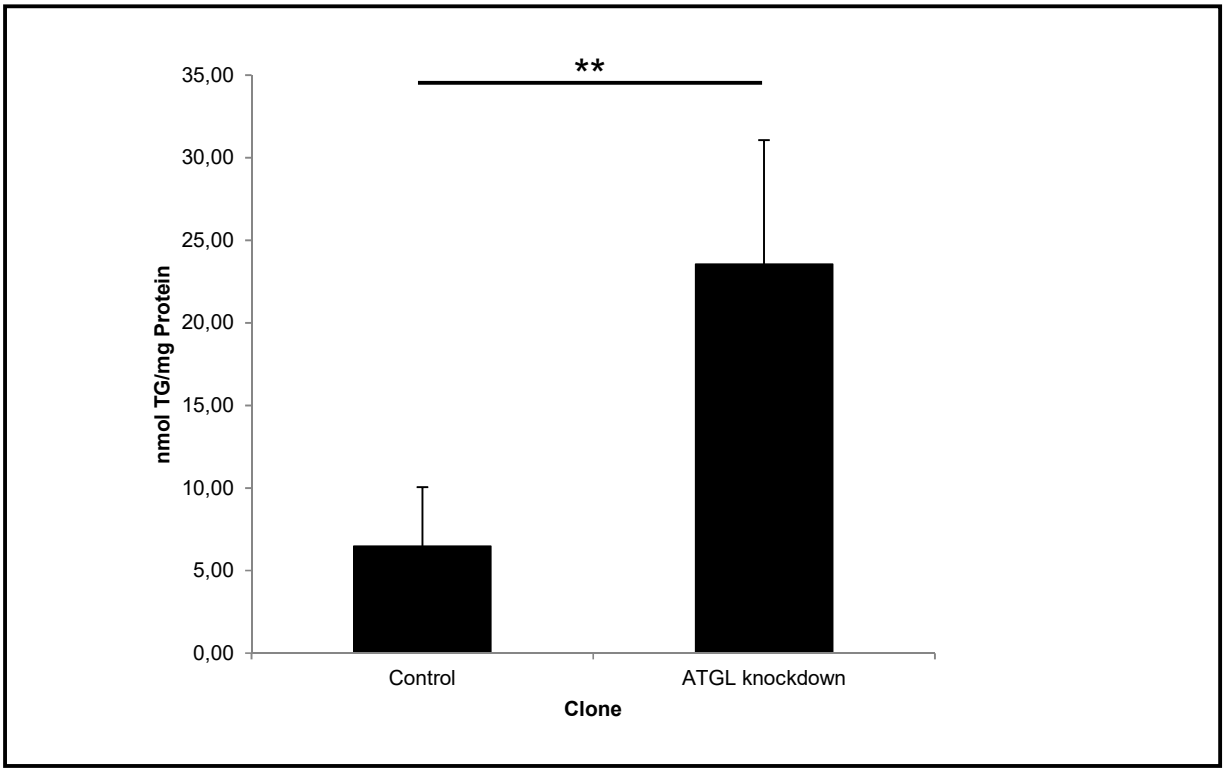

Figure 8: TG levels in myogenic differentiated C2C12 cells. After the C2C12 cells were grown to confluence, the DMEM high glucose media containing 20% FCS was replaced by a 2% FCS media to induce myogenic differentiation. Lipid was isolated with hexane-isopropanol (3:2) after 8 days in culture and quantified using Infinity™ Triglycerides Liquid Stable Reagent. Error bars represent standard error of the mean, n=3. ** $p < 0.01$.

Fluorescence microscopy of myogenic differentiated cells

Fluorescence microscopy was applied to study morphological differences between C2C12 cells depending on ATGL expression levels. In particular we focused on alterations during myogenic differentiation. For that purpose, C2C12 cells were grown in 8-well chamber slides and myogenic induction media was used to induce differentiation. Fixation of the cells was done on day 1,4 and 6 after induction. To follow cell development, anti-α-Actinin and anti-Pax7 antibodies were used to detect specific markers of myogenic differentiation. Fluorescence microscopy pictures were taken using a confocal laser scanning microscope. Clone 002 was chosen as a representative control sample, whereas clone 774 was chosen to represent C2C12 cells silenced for ATGL.

The pictures taken during different stages of differentiation show no difference in morphology between the cell samples (Figure 9). Both exhibit a roundish shape on day 1 when the overlay pictures are considered. With regard to day 4, both control and knockdown samples show tube

like structures and an increased α-Actinin signal. Even more so on day 6, supporting the notion, that ATGL knockdown doesn't negatively affect myogenic C2C12 differentiation. A gain in α-Actinin during myogenic differentiation is expected, since plenty of sarcomeres arise. Pax7 protein amount obviously has reached its minimal level in C2C12 myoblasts and thus doesn't decline any further.

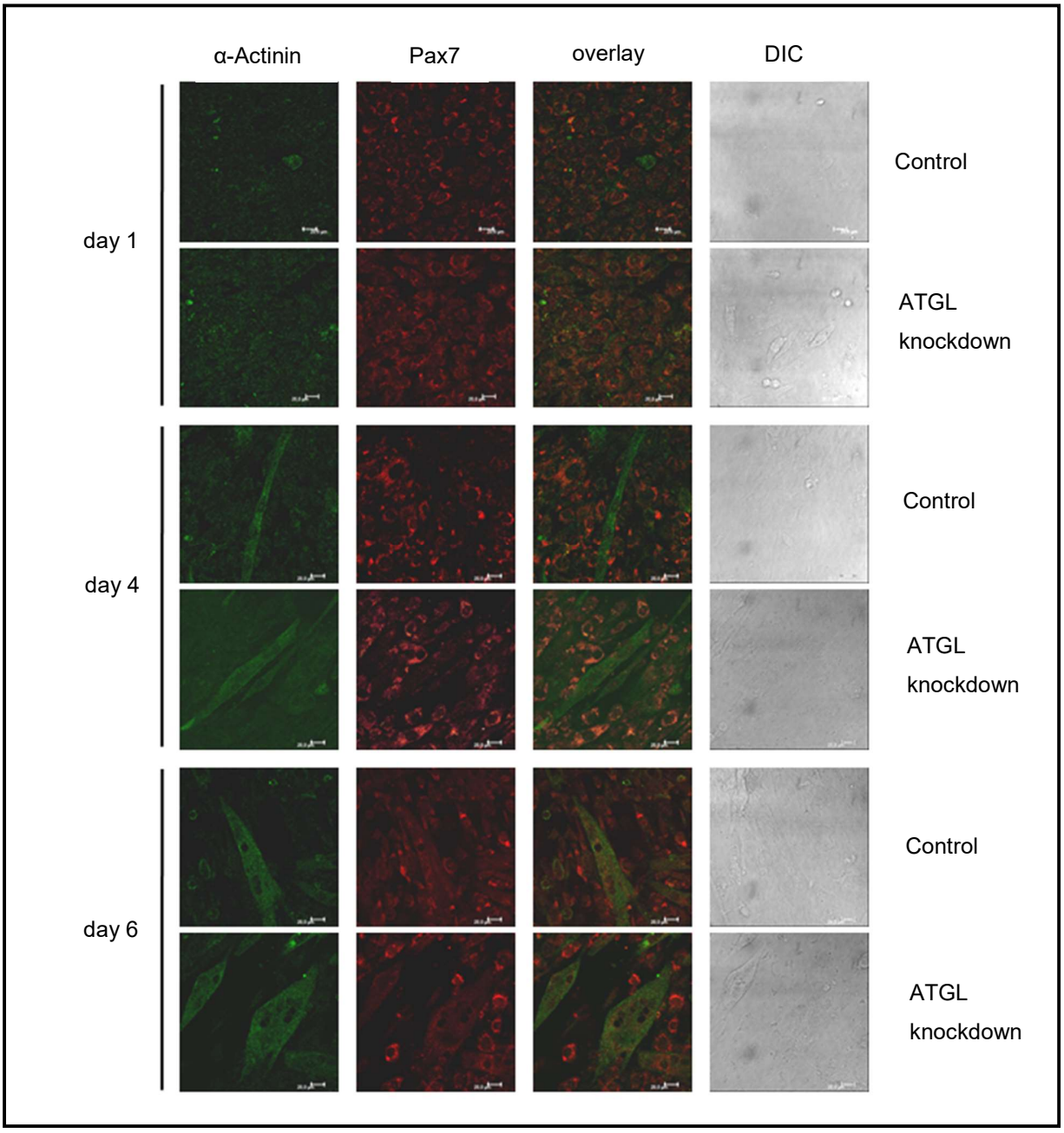

Figure 9: Fluorescence microscopy pictures of myogenic differentiated C2C12 cells. Clone 002 was chosen as a representative control sample (Control), whereas clone 774 was chosen to represent C2C12 cells silenced for ATGL (ATGL knockdown). After the C2C12 cells grown in 8-well chamber slides reached confluence, DMEM high glucose media containing 20% FCS was replaced by a 2% FCS media to induce myogenic differentiation. At indicated time points cells were fixed with formaldehyde, followed by antibody treatment and confocal fluorescence microscopy.

5.1.3 Adipogenic differentiation properties of ATGL silenced C2C12 myoblasts

After we could show that reduced ATGL levels had no negative impact on myogenic differentiation of C2C12, the experimental setup was modified to elucidate adipogenic differentiation capabilities. For this purpose, C2C12 were seeded in 6-well plates and grown in DMEM high glucose media with 20% FCS. After reaching confluence, the media was substituted by adipogenic induction media consisting of DMEM high glucose media with 10% FCS, 10 µg/ml insulin, 1 µM dexamethasone, 2 µM rosiglitazone and 0.5 mM IBMX. On day 4 the adipogenic induction media was replaced by adipogenic maintenance media consisting of DMEM high glucose media with 10% FCS, 10 µg/ml insulin and 2 µM rosiglitazone. As in the previous setup, cells were harvested at days 0,2,4,6 and 8 of differentiation. Unlike during myogenic differentiation, the clones 774 and 777 behaved unequal while adipogenic differentiation was performed. This required a discrete analyzation of the data. Therefore both clones are mentioned separately.

mRNA levels of differentiation markers

Since adipogenic Protein 2 (aP2/FABP4) increases during adipocyte formation, this marker was surveilled during adipogenic differentiation. As shown in Figure 10 A, mRNA level increased over 2000-fold in cells of clone 774, implying a greater adipogenic differentiation capability than the control, which increased its aP2/FABP4 mRNA about 1000-fold. With an 500-fold increase clone 777 couldn’t reach the levels of control.

To verify the adumbrations, stearoyl-CoA desaturase-1 (SCD1) levels were analyzed (Figure 10 B). SCD1 expression increases during adipocyte formation, where the enzyme is involved in lipid synthesis. The data showed a replication of the previous trend. Clone 774 increased SCD1 expression 15-fold, whereas the control accomplished a 5-fold gain over the 8 day period. Therefore the knockdown clone displays a superior adipogenic differentiation capability. Clone 774 showed a lower (4-fold) increase in SCD1 mRNA expression than the control.

Finally the course of PPARγ2 expression was determined during differentiation (Figure 10 C). This TF is an important regulator for the differentiation of adipocytes. Regarding the results, all clones in the experiment showed a clear peak at day 4 with a 120-fold increase for clone 774, a 50-fold for the control and a 15-fold for clone 777. This pattern matches the one previously

observed for markers aP2/FABP4 and SCD1. The summarized results show that all adipogenic markers increase during differentiation. This strongly indicates that at least some cells turned into white adipocytes during the adipogenic differentiation procedure.

Since morphological evaluation of the cultured cells clearly presented myogenic tubes during adipogenic differentiation, we also checked myogenic markers. As illustrated in Figure 11 A, MHC2B mRNA level increase for clone 774 (25000-fold), clone 777 (17000-fold) and control (14000-fold). As with PPARγ2, the trend shows a peak at day 4.

The trend seen in MHC2B is reflected by the expression of MyoD (Figure 11 B), which rose at day 4 up to 5.5-fold for clone 774, 6- fold for clone 777 and about 3.5-fold for the control. The tremendous increase of myogenic marker expression indicates that a significant part of the cells grown in adipogenic media still fullfill the myogenic cell fate.

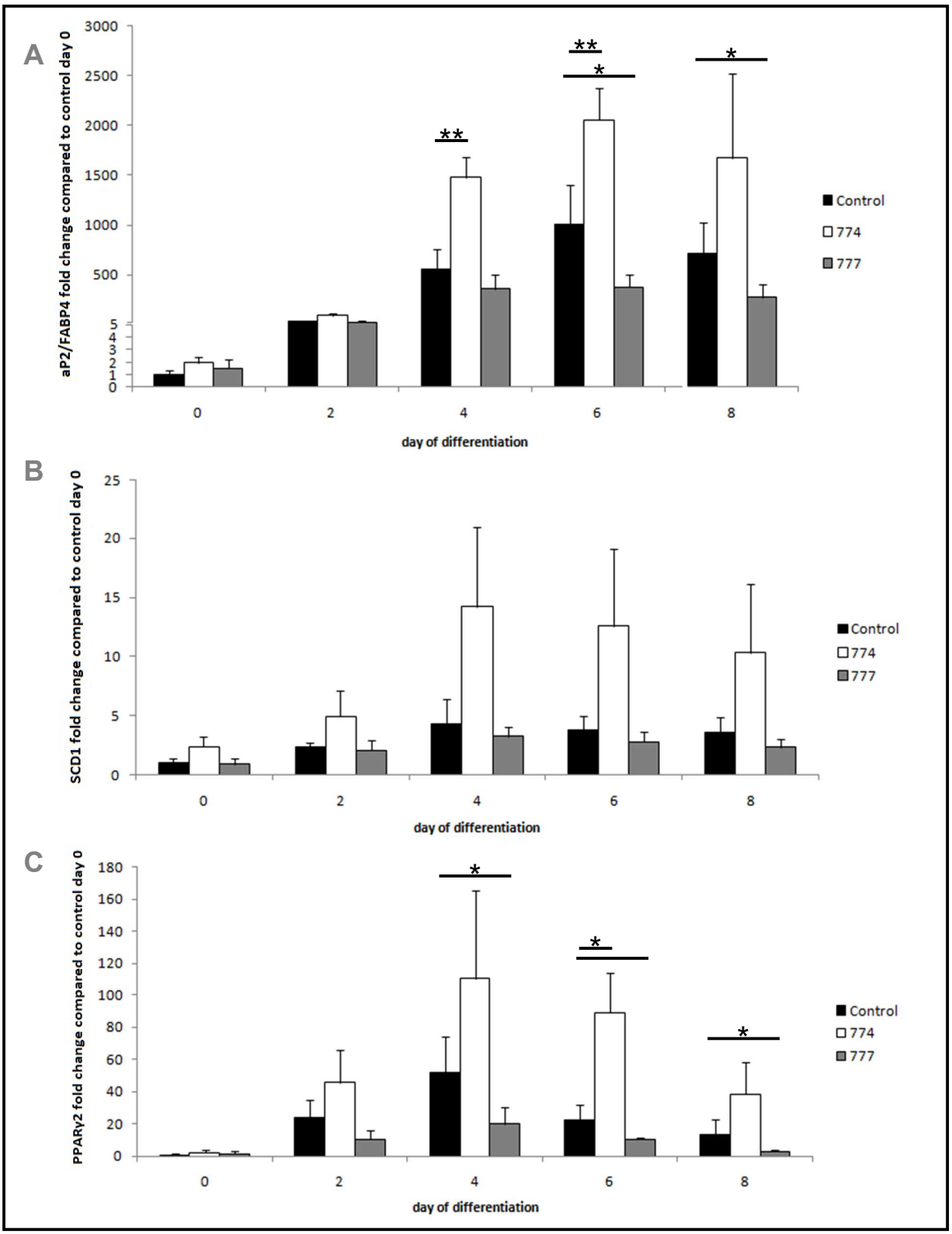

Figure 10: Gene expression of adipogenic marker genes aP2/FABP4, SCD1 and PPARγ2 during 8 days of adipogenic differentiation. After the C2C12 cells were grown to confluence, the DMEM high glucose media containing 20% FCS was replaced by adipogenic induction media containing 10% FCS, 10 µg/ml insulin, 1 µM dexamethasone, 2 µM rosiglitazone and 0.5 mM IBMX. After four days the media was replaced by adipogenic

maintenance media containing 10% FCS, 10 µg/ml insulin and 2 µM rosiglitazone. The mRNA level was determined (normalized to 1) by qRT-PCR analysis using Primers for aP2/FABP4 **(A)**, SCD1 **(B)** and PPARγ2 **(C)** genes after cells were harvested at indicated time points. Error bars represent standard error of the mean, n=3. *$p < 0.05$. **$p < 0.01$.

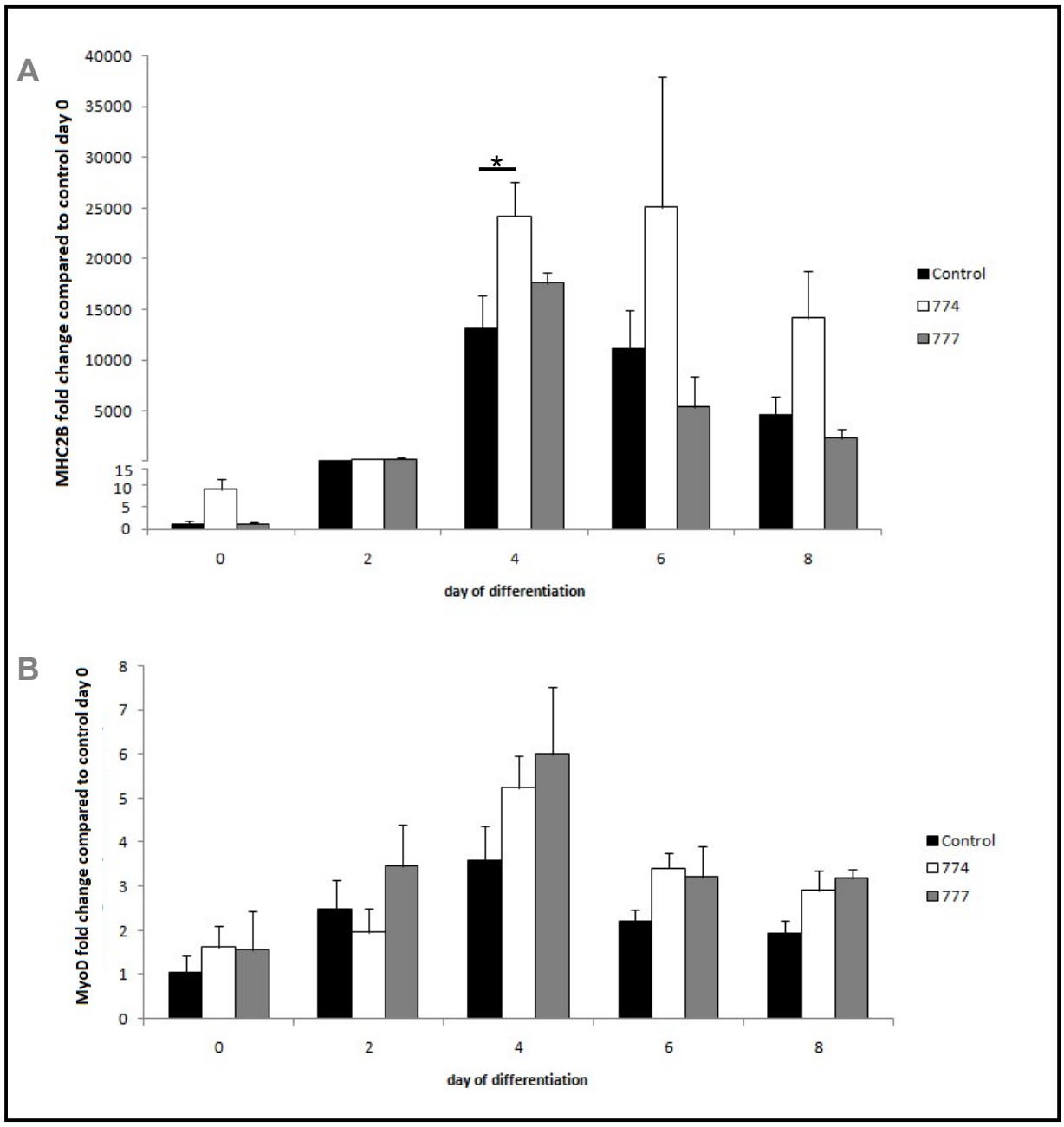

Figure 11: Gene expression of myogenic marker genes MHC2B and MyoD during 8 days of adipogenic differentiation. After the C2C12 cells were grown to confluence, the DMEM high glucose media containing 20% FCS was replaced by adipogenic induction media containing 10% FCS, 10 µg/ml insulin, 1 µM dexamethasone, 2 µM rosiglitazone and 0.5 mM IBMX. After four days the media was replaced by adipogenic maintenance media containing 10% FCS, 10 µg/ml insulin and 2 µM rosiglitazone. At indicated time points the cells were harvested and the mRNA level was determined (normalized to 1) using Primers for MHC2B **(A)** and MyoD **(B)** genes in qRT-PCR analysis. Error bars represent standard error of the mean, n=3. *$p < 0.05$.

TG levels of adipogenic differentiated cells

As observed for the myogenic differentiation, ATGL silencing also leads to increased TG accumulation in adipogenic differentiated C2C12 cells with even higher values (Figure 12). By aggregating nearly 80 nmol TG per mg Protein, clone 774 accumulates about twice as much as the control (43 nmolTG/mg Protein). Clone 777 ranged between clone 774 and the control with 58 nmol TG per mg Protein.

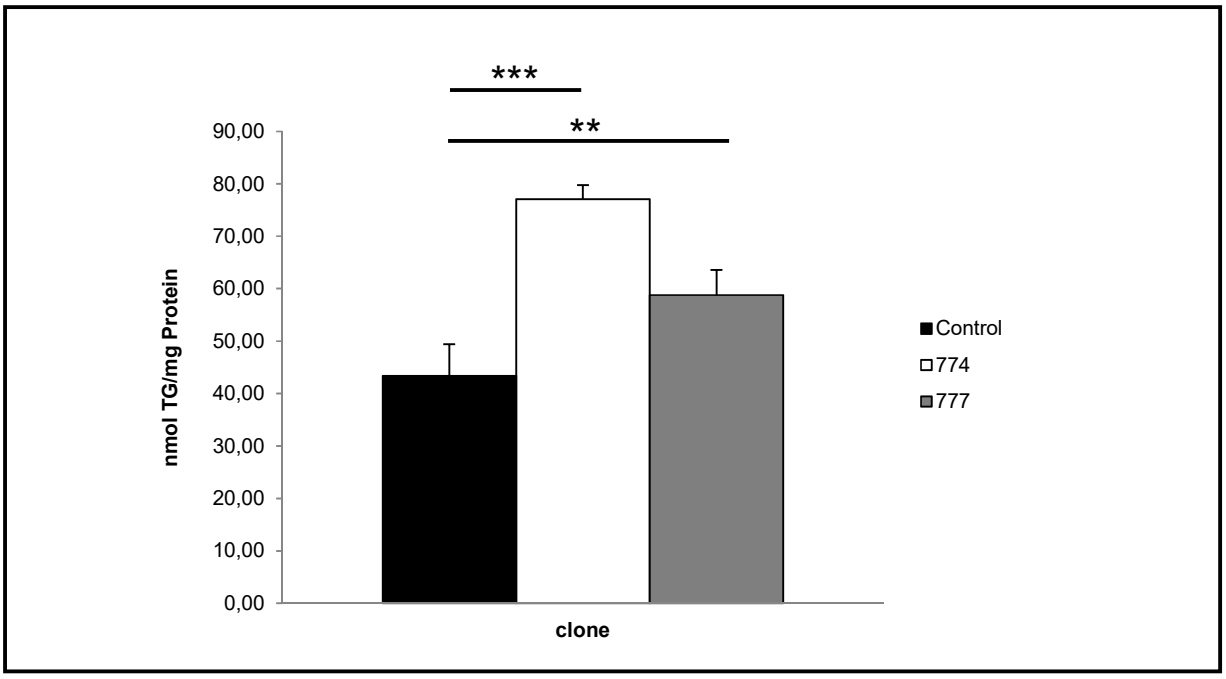

Figure 12: TG levels in adipogenic differentiated C2C12 cells. After the C2C12 cells were grown to confluence, the DMEM high glucose media containing 20% FCS was replaced by adipogenic induction media containing 10% FCS, 10 µg/ml insulin, 1 µM dexamethasone, 2 µM rosiglitazone and 0.5 mM IBMX. After 4 days the media was replaced by adipogenic maintenance media containing 10% FCS, 10 µg/ml insulin and 2 µM rosiglitazone. Lipid was isolated with hexane-isopropanol (3:2) after 8 days in culture and analyzed using Infinity™ Triglycerides Liquid Stable Reagent. Error bars represent standard error of the mean, n=3. $^{**}p < 0.01$; $^{***}p < 0.001$.

5.2 Isolation and differentiation of primary satellite cells from wild type and ATGL knockout mice

After we investigated the impact of ATGL silencing in a muscle cell line, we focused on primary cells. Therefore we set up a protocol to isolate satellite cells from mouse muscle with the effort to differentiate the obtained cells either into adipocytes or myocytes. We intended to isolate satellite cells not only from wild type mice, but also from ATGL knockout mice, to check their differentiation properties. Due to the lack of time and mice, we were not able to properly isolate cells from ATGL knockout mice. Therefore, the differentiation studies could only be performed in satellite cells of wild type mice.

5.2.1 Establishing a protocol to isolate satellite cells from mouse musculus tibialis anterior and musculus gastrocnemius

To obtain skeletal muscle samples, 4-week-old C57BL/6J mice were sacrificed. The skin was removed from the hindlimbs and tibialis anterior muscles (TA) and gastrocnemius muscles (GC) were taken. The muscles were placed on a petri dish wetted with pre-warmed DMEM/F-12 + GlutaMAX™. Tendons and connective tissue were removed under the light microscope before the muscles were chopped into small pieces (about 3 mm^3). The muscle pieces of each mouse were pooled in a 15 ml tube containing 3 ml DMEM/F-12 + GlutaMAX™. The tube was kept on 37°C till all muscles were collected.

At first, the suspension was pelleted by centrifuging with 50 g for 30 seconds at room temperature to collect the tissue pieces. The supernatant was removed and 5 ml DMEM/F-12 + GlutaMAX™ with 0.14% pronase from *Streptomyces griseus* (Sigma-Adlrich, St. Louis, USA) was added to loosen the cells. After 10 minutes of incubation with frequent mixing, the tissue pieces were centrifuged with 400 g for 30 seconds at room temperature. Afterwards, the supernatant mainly containing fibroblasts was discarded and 5 ml DMEM/F-12 + GlutaMAX™ with 20% FCS and 2% Ultroser™ G (Pall, Port Washington, USA) was added to the pellet. A sterile 5 ml pipette was used to loosen the cells out of the tissue pieces, by passing the suspension 20 times vigorously through the pipette tip. Centrifugation at 400 g for 30 seconds generated the supernatant containing satellite cells. The supernatant was transferred into a 50 ml tube where 25 ml DMEM/F-12 + GlutaMAX™ with 20% FCS and 2% Ultroser™ G was present. The cycle was repeated two times from the point where fresh DMEM/F-12 + GlutaMAX™ media with 20% FCS and 2% Ultroser™ G was added to the tissue pieces.

Afterwards, the supernatant was combined with the supernatant from the previous cycle in the 50 ml tube. After three rounds the collected cell suspension was passed through a sterile 70 µm cell strainer into a new 50 ml tube, followed by centrifugation for 5 minutes at 400 g and room temperature. The supernatant was discarded and the cell pellet was resuspended in 10 ml DMEM/F-12 + GlutaMAX™ with 20% FCS and 2% Ultroser™ G. After a final centrifugation for 5 minutes at 400 g and room temperature, the supernatant was removed again. The pellet was resuspended in 100 µl DMEM/F-12 + GlutaMAX™ with 20% FCS and 2% Ultroser™ G.

10 µl of the cell suspension were counted under the light microscope, using a Neubauer cell counting chamber (Brand GmbH & Co. KG, Wertheim, Germany). Only refractive cells with roundish shape were counted. Cells were seeded in gelatin coated 12-well plates at a density of 5000 cells per well. The provided DMEM/F-12 + GlutaMAX™ with 20% FCS and 2% Ultroser™ G media was changed every other day. Figure 13 shows a picture taken from isolated cells. Many satellite cells have differentiated into myotubes upon high density or the altered environment lacking regulatory factors. To avoid the differentiation and increase the satellite cell purity, a clonally expansion was performed.

For this purpose, the cells were washed with 1x PBS and detached using Gibco® Trypsin-EDTA (Thermo Fisher Scientific Inc., Waltham, USA). To stop trypsinization after 30 seconds, some media was added. The cell solution was transferred into a tube and centrifuged for 3 minutes at 400 g. After the supernatant was removed, the cell pellet was resuspended in DMEM/F-12 + GlutaMAX™ with 20% FCS and 2% Ultroser™. In the next step cells were counted using a Neubauer cell counting chamber. The cells were then diluted and seeded into gelatin coated 96-well plates. To end up with clonal satellite cells, the dilution was performed in a way, that statistically only one cell is seeded into a well. The growth was monitored till wells appeared that contained single satellite cells colonies. These cells were propagated in gelatin coated 12-well plates. To prevent confluence they were transferred to coated 6-well plates in the next step. Afterwards, they were cultured in coated flasks. When cells reached higher densities in 175 cm² flasks, they were seeded into coated 6-well plates and the differentiation experiments were performed.

The isolation with the denoted protocol was done with wild type and ATGL knockout mice. During the experiment only the wild type cells engrafted properly and could be propagated further. Satellite cells isolated from knockout mice didn’t expand and were therefore overgrown

by fibroblast. Hence, the differentiation experiment could only be performed with satellite cells isolated from wild type mice.

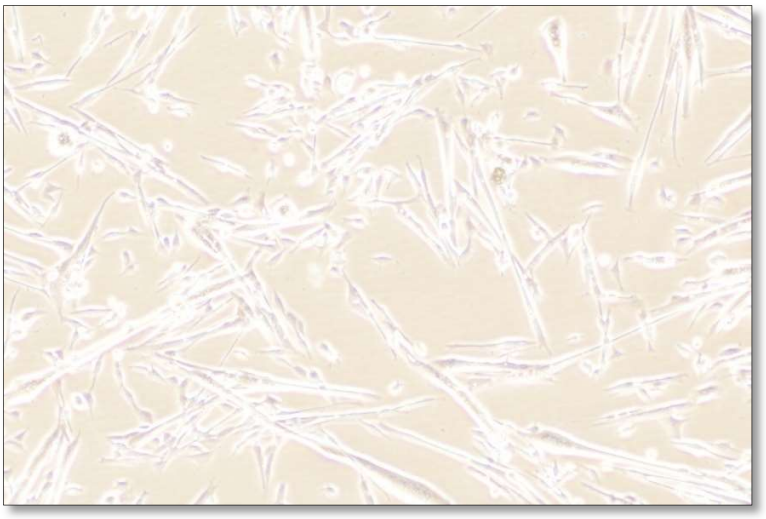

Figure 13: DIC picture of 6 days cultured cells after isolation from wild type mouse TA and GC. The cells were isolated according to the protocol and cultured in gelatin coated 12-well plates with DMEM/F-12 + GlutaMAX^{TM} media containing 20% FCS.

5.2.2 Myogenic and adipogenic differentiation properties of satellite cells isolated from wild type mice

ATGL expression in primary muscle cells during myogenic and adipogenic differentiation

After it could be shown that ATGL gene expression increases up to 3.5-fold during myogenic differentiation in non silenced C2C12 cells (see 5.1.1), we wanted to investigate whether this holds also true for primary muscle stem cells. Figure 14 shows that also in primary cells ATGL mRNA level rise by 3.5-fold and 2.5-fold during myogenic and adipogenic differentiation, respectively.

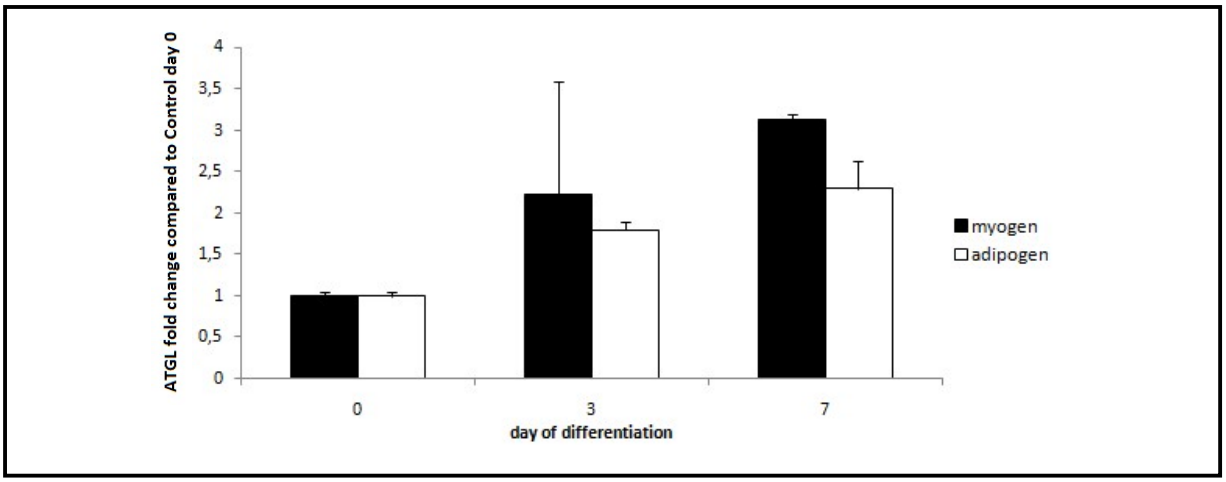

Figure 14: ATGL mRNA level of myogenic and adipogenic differentiated satellite cells isolated from mouse muscle. After the cells were isolated according to the protocol, a clonal expansion of satellite cells was performed to get rid of fibroblasts. The obtained cells were cultured in gelatin coated 6-well plates till confluence, when myogenic and adipogenic differentiation was induced by myogenic media (DMEM/F-12 + GlutaMAX^{TM} with 2% FCS) and adipogenic media (DMEM/F-12 + GlutaMAX^{TM} with 10% FCS, 10 µg/ml insulin, 1 µM dexamethasone, 2 µM rosiglitazone and 0.5 mM IBMX). After the cells were harvested at indicated time points, qRT-PCR was performed to determine ATGL gene expression (normalized to 1). Error bars represent standard error of the mean, n=2.

Myogenic marker expression during myogenic and adipogenic differentiation of primary muscle cells

To evaluate the differentiation capabilities of the satellite cells, MHC2B and MyoD gene expression was determined by qRT-PCR. The analysis was performed after seven days of myogenic and adipogenic differentiation. In both differentiation protocols, cells primarily adopted the myogenic fate as proven by the increase of MHC2B levels up to 22-fold in myogenic and 11-fold in adipogenic differentiated cells (Figure 15 A).

MyoD levels dropped about 50% in myogenic and 80% in adipogenic differentiated cells during the 7 days (Figure 15 B). This indicates that the cells already expressed high levels of the early TF at the beginning of the experiment, probably due to elevated cell density. Hence, the measured trend illustrates an advanced differentiation state where MyoD gene expression is returning to a basal level. MyoD levels notably decrease further in adipogenic differentiated cells, indicating a condition with lesser commitment towards the myogenic fate.

The canonical satellite cell marker Pax7 expressed in isolated primary muscle cells decreased its mRNA level over 80% during differentiation, confirming the isolated cells to be satellite cells (Figure 15 C).

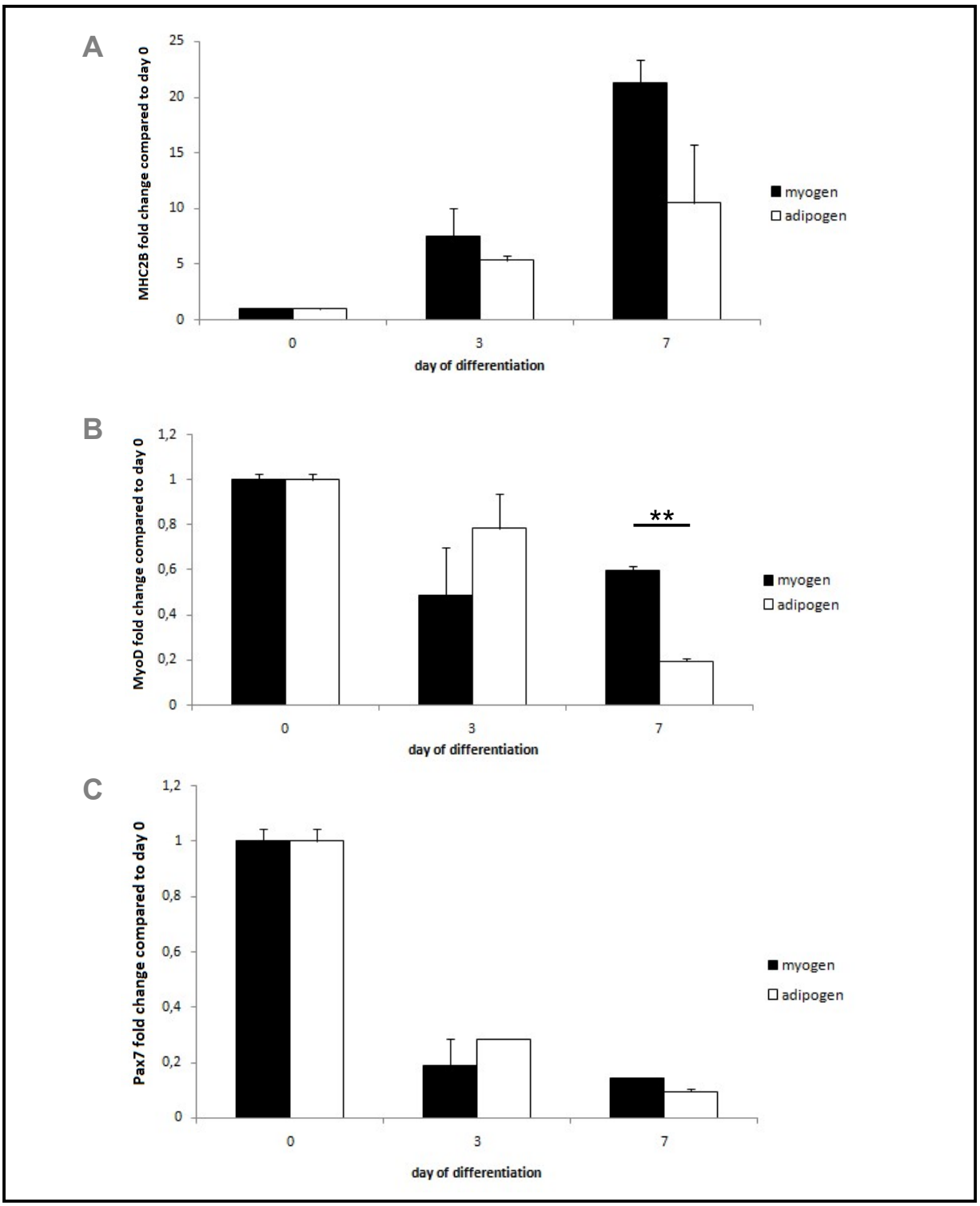

Figure 15: Myogenic marker gene expression of myogenic and adipogenic differentiated satellite cells isolated from mouse muscle. After cells were isolated according to the protocol, a clonal expansion of satellite cells was performed to get rid of fibroblasts. Cells were cultured in gelatin coated 6-well plates till confluence, when myogenic and adipogenic differentiation was induced by myogenic media (DMEM/F-12 + GlutaMAX™ with 2% FCS) and adipogenic media (DMEM/F-12 + GlutaMAX™ with 10% FCS, 10 µg/ml insulin, 1 µM dexamethasone, 2 µM rosiglitazone and 0.5 mM IBMX). After the cells were harvested at indicated time points, qRT-PCR was performed to determine gene expression of MHC2B **(A)**, MyoD **(B)** and Pax7 **(C)** (normalized to 1). Error bars represent standard error of the mean, n=2. $^{**}p < 0.01$.

Adipogenic marker expression during myogenic and adipogenic differentiation of primary muscle cells

As done for C2C12 cells, primary cells were also subjected to myogenic and adipogenic differentiation. To confirm adipocyte formation the adipogenic marker aP2/FABP4 was determined. Cells which where incubated in myogenic media reduced aP2/FABP4 gene expression over 99% during 7 days in culture, cells in adipogenic media about 95% (Figure 16). The fact that primary cells in adipogenic media maintained slightly higher aP2/FABP4 expression levels than cells in myogenic media indicates that at least some adipocytes could have been formed while the adipogenic differentiation was performed.

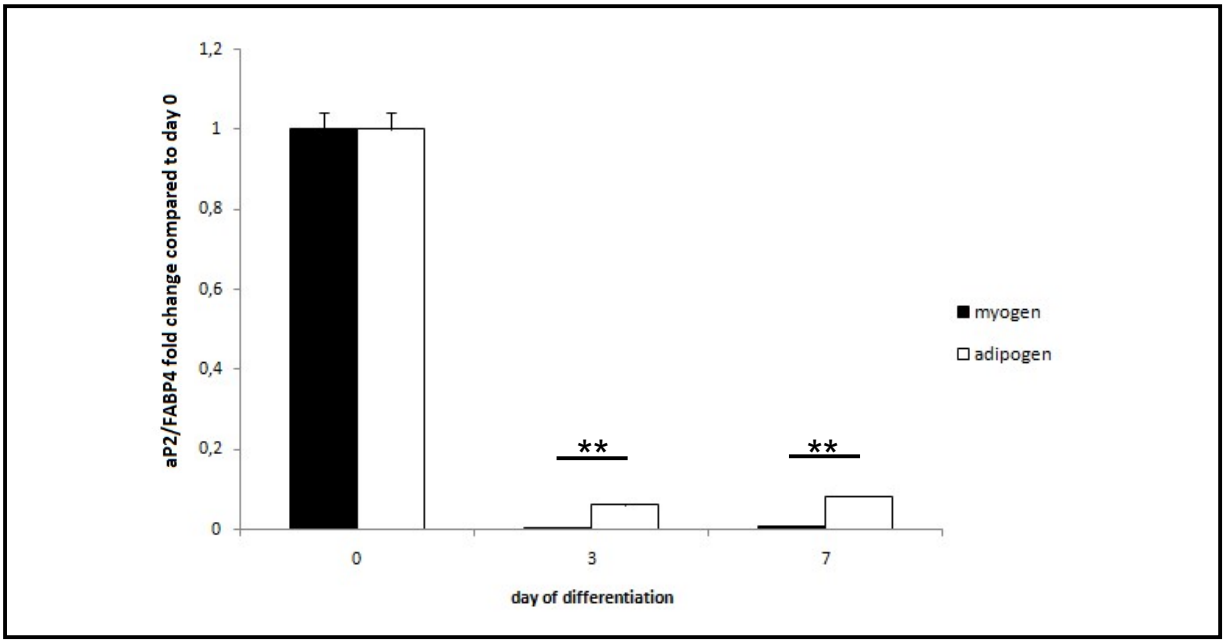

Figure 16: aP2/FABP4 expression levels of myogenic and adipogenic differentiated satellite cells isolated from mouse muscle. After the cells were isolated according to the protocol, a clonal expansion of satellite cells was performed to get rid of fibroblasts. The obtained cells were cultured in gelatin coated 6-well plates till confluence when myogenic and adipogenic differentiation was induced by myogenic media (DMEM/F-12 + GlutaMAX^{TM} with 2% FCS) and adipogenic media (DMEM/F-12 + GlutaMAX^{TM} with 10% FCS, 10 µg/ml insulin, 1 µM dexamethasone, 2 µM rosiglitazone and 0.5 mM IBMX). After the cells were harvested at indicated time points, qRT-PCR was performed to determine P2/FABP4 gene expression (normalized to 1). Error bars represent standard error of the mean, n=2. $^{**}p < 0.01$.

5.3 The influence of ATGL on mouse muscle during ageing

It is well known that protein levels of certain genes can vary significantly during aging through up- and downregulation of gene expression. To investigate whether *ATGL* expression is also regulated by ageing in skeletal muscle, tissue samples of young (4 months) and old (19 months) mice were analyzed. Furthermore it was examined whether lipid accumulation or any signs of muscle damage appear in correlation with altered ATGL levels during aging.

5.3.1 ATGL levels in young and aged mouse muscle

ATGL gene expression in young and aged mouse muscle

The ATGL gene expression in quadriceps femoris muscle of young mice matches the expression determined in old mice (Figure 17).

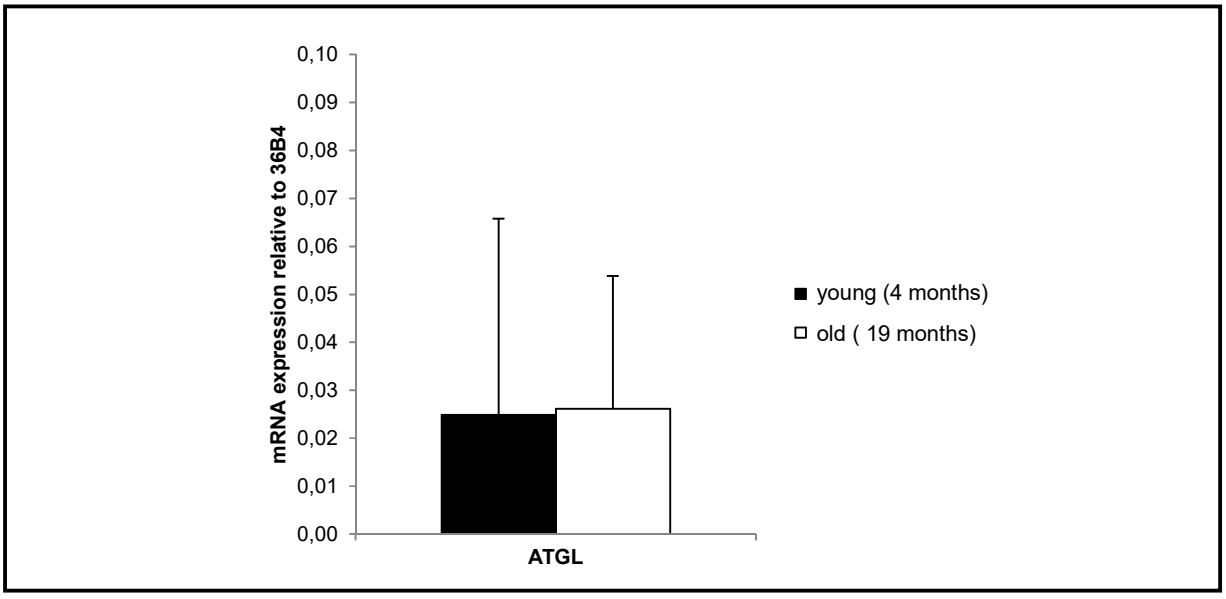

Figure 17: ATGL expression in quadriceps femoris muscle of young and old mice. Frozen quadriceps femoris muscle was powderized and mRNA was isolated (see 4.2.3), followed by qRT-PCR analysis using primers for ATGL. Error bars represent standard error of the mean.

ATGL protein amount in young and aged mouse muscle

As shown in Figure 18, ATGL protein levels didn't change during aging, since young (4 months) and old (19 months) exhibit almost the same amount of protein. Combined with the unaltered *ATGL* expression in aged mice, these results indicate a constant ATGL level throughout lifetime.

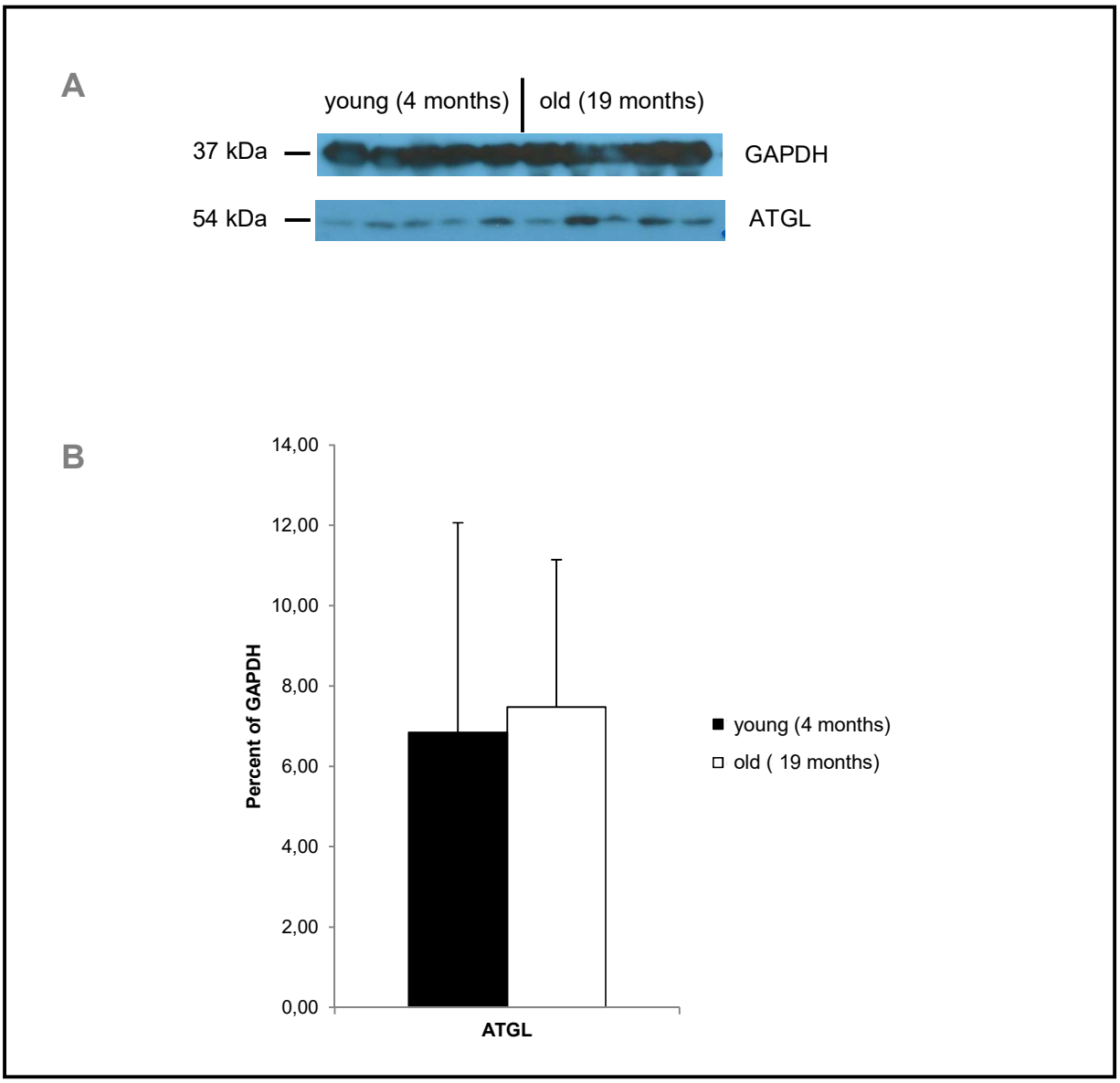

Figure 18: ATGL protein level in quadriceps femoris muscle of young and old mice. Frozen quadriceps femoris muscle was powderized and protein was isolated (see 4.4.1). 50 µg protein lysate was used for western blot analysis **(A)** (see 4.4.6). GAPDH was used as the loading control. Blots were scanned and image analysis was performed using Quantity One® 1-D analysis software **(B)**. Error bars represent standard error of the mean.

5.3.2 TG levels in mouse muscle of young and aged mice

Lipid accumulation during ageing may be caused by defective lipolysis due to reduced ATGL activity, therefore we determined TG levels in quadriceps muscle of young and old mice. Figure 19 illustrates, that old mice do not accumulate TGs compared to young mice. With about 75 nmol TG per mg protein, old mice tend to have as much TGs as young mice (95 nmol TG/mg protein). This is in line with unaltered ATGL abundance, hypothesizing constant TG levels in mouse muscle during aging.

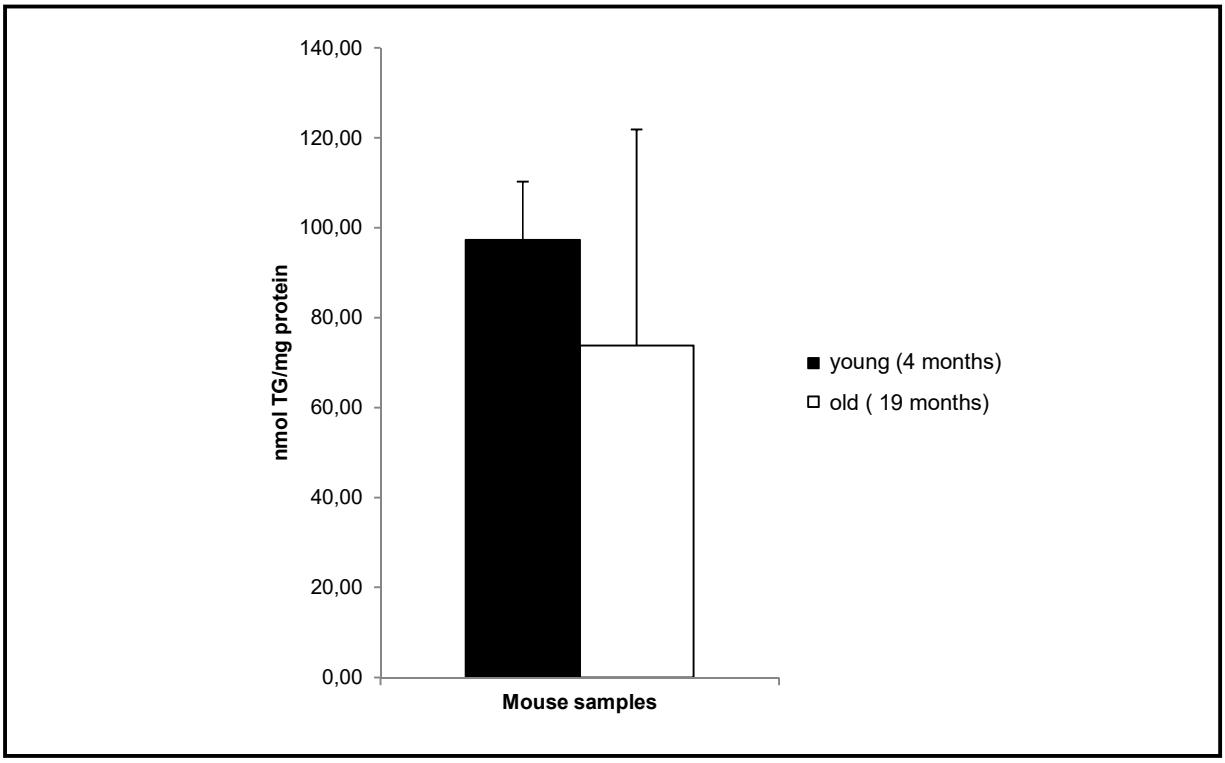

Figure 19: TG level in quadriceps femoris muscle of young and old mice. Frozen quadriceps muscle tissue was powderized and lipids were isolated using the method of Folch (see 4.3.2). The measurement was performed with Infinity™ Triglycerides Liquid Stable Reagent (see 4.3.3). Error bars represent standard error of the mean.

5.3.3 Atrophy marker levels compared in young and aged mouse muscle

Besides ATGL abundance, old mice were examined for signs of muscle damage. Therefore expression levels of LC3B, MuRF-1 and Atrogin-1 were determined.

Protein level of atrophy marker LC3B in young and aged mouse muscle

Increased levels of LC3BII, a modified form of LC3B, appears during autophagy and can be assessed as marker for cell damage. The analysis showed that the amount of LC3BII was three times lower in older than in younger mice (Figure 20), suggesting catabolic processes weren't prevalent.

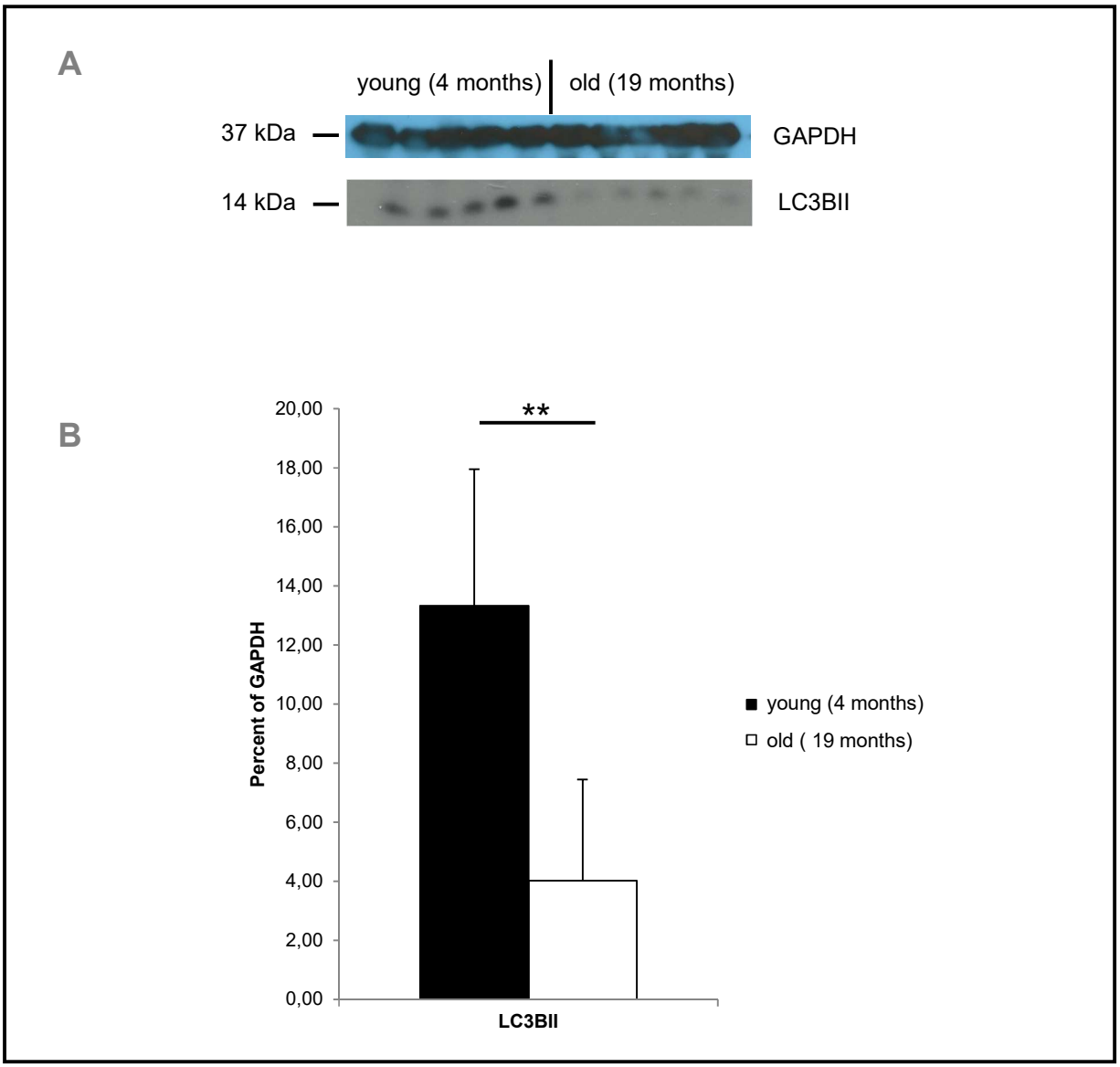

Figure 20: LC3BII protein level in quadriceps femoris muscle of young and old mice. Frozen quadriceps muscle was powderized and protein was isolated (see 4.4.1). 50 µg protein lysate was used for western blot analysis **(A)** (see 4.4.6). GAPDH was used as the loading control. Blots were scanned and image analysis was performed using Quantity One® 1-D analysis software **(B)**. Error bars represent standard error of the mean. $^{**}p < 0.01$.

Gene expression of atrophy markers in young and aged mouse muscle

Muscle atrophy was further evaluated by gene expression levels of E3 ubiquitin ligases MuRF-1 and Atrogin-1. During cell damage ubiquitin ligases route proteins towards the proteasomal degradation pathway and are therefore expressed in greater quantities. Figure 21 shows that mRNA levels of both ligases tend to drop slightly in aged mice, fortifying the assumption, that old mice don't show muscle damage or atrophy.

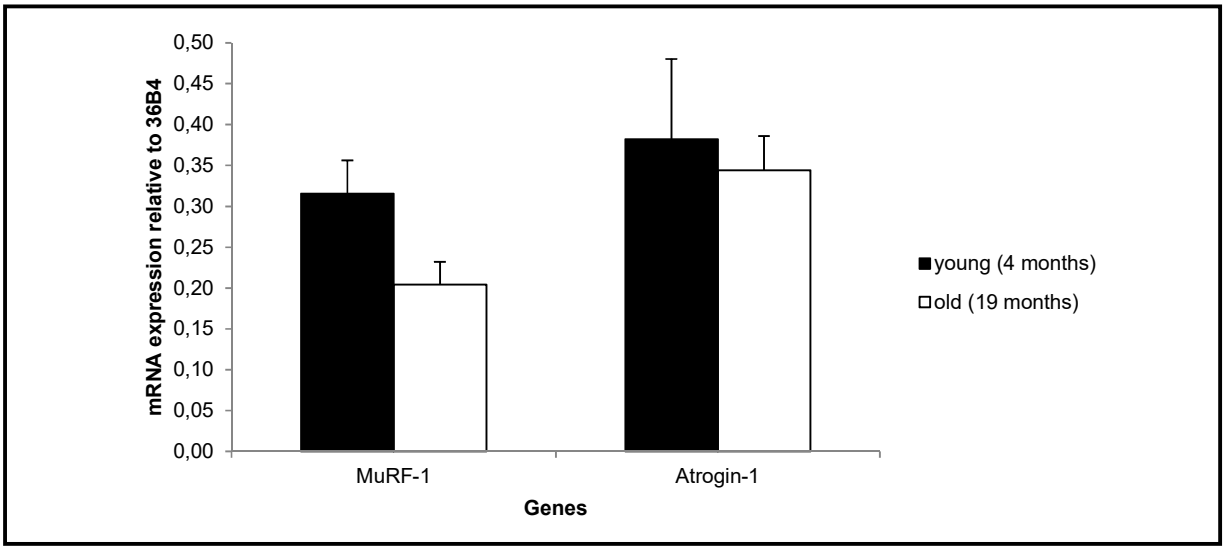

Figure 21: Gene expression levels of cell damage marker MuRF-1 and Atrogin-1 in quadriceps femoris muscle of young and old mice. Frozen quadriceps muscle was powderized and mRNA was isolated (see 4.2.3), followed by qRT-PCR analysis using primers for MuRF-1 and Atrogin-1. Error bars represent standard error of the mean.

5.4 Induction of muscle damage by glycerol injection into mouse muscle

In nephrology studies glycerol was used to induce acute renal failure (80). Besides this area of application, it was recently reported that glycerol injections into skeletal muscle lead to muscle damage with adipocyte formation during the recovery (75). To ascertain whether ATGL plays a role in the development of intramuscular adipocytes, it was intended to inject glycerol into gastrocnemius muscle (GC) and tibialis anterior muscle (TA) of wild type and ATGL knockout mice. After 4 weeks the mice were sacrificed and muscular adipocyte markers as well as the TG content was analyzed.

5.4.1 Establishing a glycerol injection protocol to induce mouse muscle damage

The glycerol injection model was performed with 12-week-old wild type C57BL/6J mice. Mice were anesthetized with 80 µg/g Ketamidor (Richter Pharma AG, Wels, Austria), 8 µg/g Rompun®TS (Bayer HealthCare, Leverkusen, Germany) and placed on a 37°C heating plate to prevent cooling. Both hindlimbs were depilated before 25 µl 50% glycerol in 1x PBS was injected in TA and GC of one hindlimb. As control, 25 µl 1x PBS was injected in TA and GC of the second hindlimb. After 4 weeks mice were sacrificed, TA and GC muscles were taken and frozen at -80°C. The following steps including muscle tissue powderization, RNA and lipid isolation as well as the qRT-PCR and lipid determination were performed as denoted in the methods part (4.2 & 4.3).

5.4.2 TG levels in glycerol injected mouse muscle

The analyzed GC muscles of glycerol injected wild type mice displayed no increased TG accumulation, which would indicate adipocyte formation (Figure 22). With 45 nmol TG per mg protein, glycerol injected mice exhibited lower lipid amounts than the control (55 nmol TG/mg protein), implying that the experiment could not generate intramuscular adipocytes and needs to be further optimized. Since TA muscles were smaller in size, the whole sample was used up during adipocyte marker analysis and TG content was therefore only determined in GC muscles.

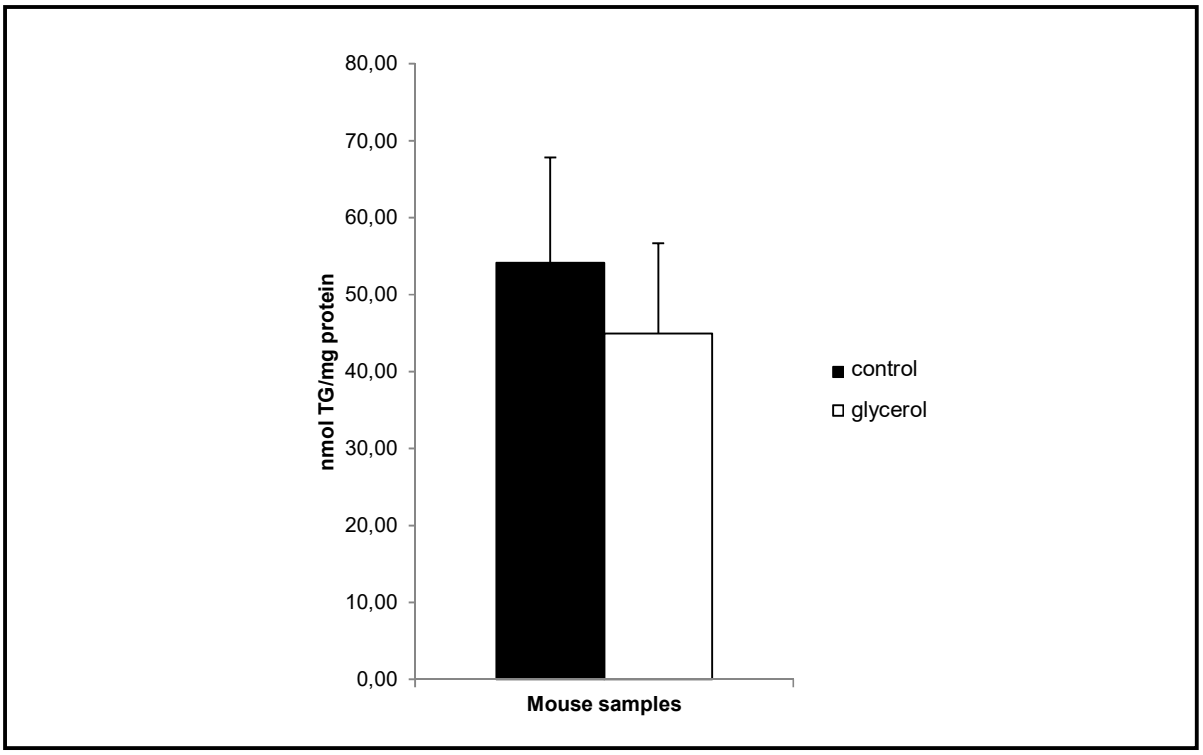

Figure 22: TG level of glycerol injected mouse gastrocnemius muscle. Glycerol and PBS (control) was injected into TA and GC muscle of wild type mice. After 4 weeks mice were sacrificed and the muscles taken. GC muscles were powderized and the lipids isolated (see 4.3.2). TG content was measured using InfinityTM Triglycerides Liquid Stable Reagent. Error bars represent standard error of the mean.

5.4.3 Adipocyte RNA marker level in glycerol injected mouse muscle

The main basis for the evaluation of a successful adipocyte formation comprised the determination of adipocyte marker gene expression. As reliable markers PPARγ2, FABP4 and SCD1 were analyzed in TA and GC of glycerol injected wild type mice.

The ascertained data for TA muscles showed increased levels for all three markers (Figure 23 A). PPARγ2 gene expression was about 2-times higher after four weeks, SCD1 even 3-times, in comparison to the control. FABP4 expression was about 20% higher than the control. Taken together, adipocyte formation in TA muscle can be supposed, but not fortified by the TG status. The latter couldn't be determined due to low sample quantity.

Figure 23 B shows, that in contrast to TA, the markers displayed slightly lower gene expression levels in glycerol injected GC muscles than in PBS injected muscles. PPARγ2 and SCD1 mRNA levels were about 20% lower than the control, FABP4 about 15%. As indicated by the unaltered TG levels in glycerol injected GC muscle (see 5.4.2), marker gene expression concurs with the notion that the experiment requires further optimization to generate adipocytes.

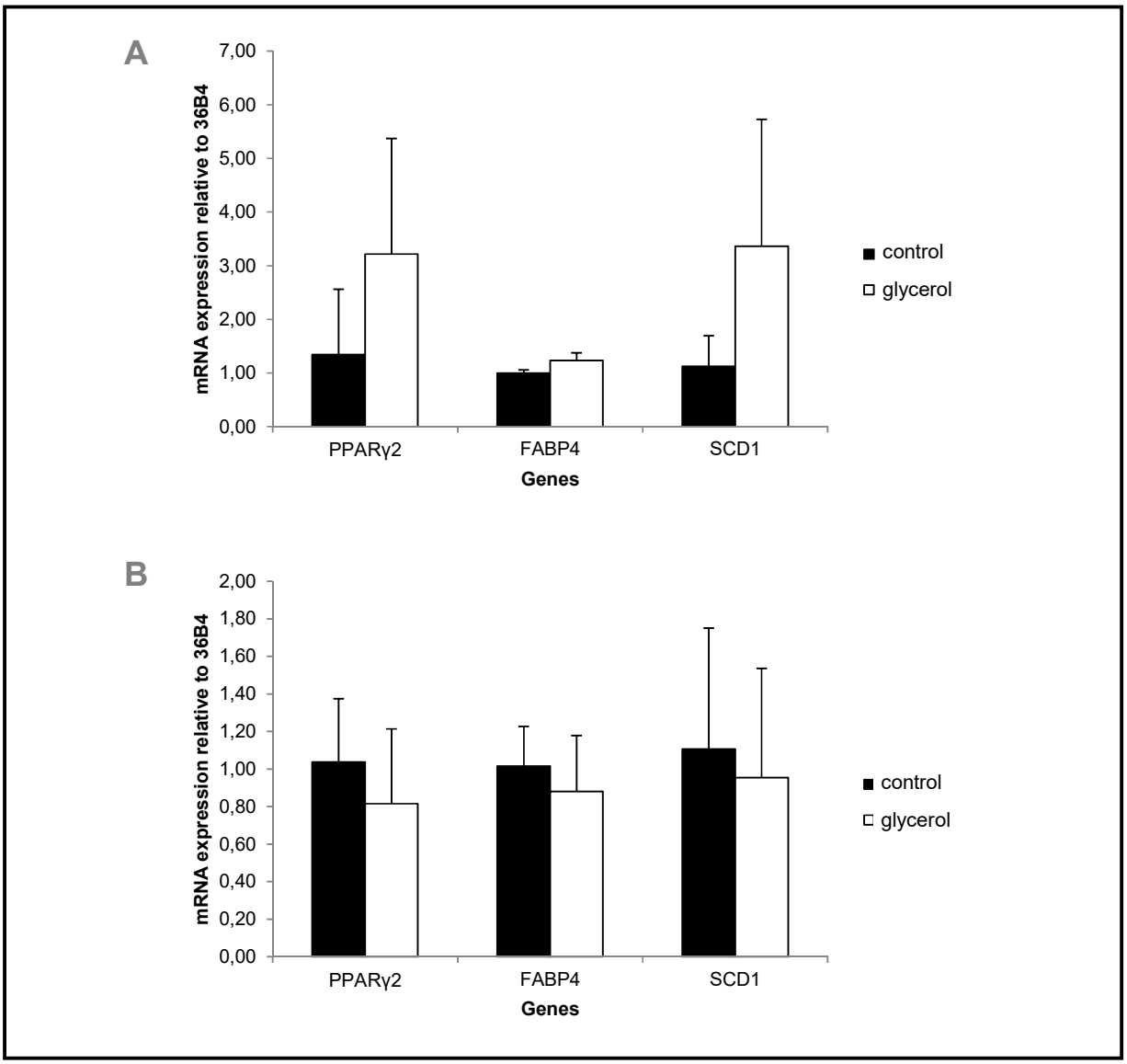

Figure 23: Gene expression levels of adipocyte markers PPARγ2, FABP4 and SCD1 in glycerol injected mouse muscle. Glycerol and PBS (control) were injected into TA and GC muscle of wild type mice. After 4 weeks mice were sacrificed and the muscles excised. Frozen TA **(A)** and GC **(B)** muscles were powderized and RNA isolated (see 4.2.3). Gene expression (normalized to 1) was determined by qRT-PCR using primers for PPARγ2, FABP4 and SCD1. Error bars represent standard error of the mean.

6 Discussion

Regeneration capabilities are a crucial feature of skeletal muscles. During day-to-day activites, heavy exercise or different states of disease, myofibers of the muscle get damaged. The coordinated proliferation and fusion of muscle stem cells is central for healing processes reconstituting muscle integrity. The consequence of a disturbed regeneration response is the loss of muscle mass accompanied by muscle weakness. A common characteristic associated with muscle degenerative processes is the development of ectopic fat within the muscle, termed IMAT.

Patients suffering from NLSDM show symptoms of muscle atrophy and reduced muscle strength. The connection between a deficiency in the fat mobilizing enzyme ATGL and the occurrence of muscle degeneration has not been fully understood. Unpublished data from the group of Matthijs Hesselink[2] showed that the myogenic differentiation process of satellite cells isolated from NLSDM patients is severely impaired. The plausible assumption that skeletal muscle loss is provoked through insufficient supply of myoblasts fusing to damaged myofibers prompted us to perform a cell culture experiment. Therefore, lentiviral siRNA mediated knockdown of ATGL in C2C12 mouse myoblasts was performed to show whether these cells fail to differentiate into myotubes upon the administration of myogenic media.

We found that C2C12 cells lacking ATGL differentiate properly into myotubes upon induction of myogenic differentiation. Morphological analysis by fluorescence microscopy showed that there was no difference between ATGL knockdown and control cells concerning tube amount or size. This could be further confirmed by the gene expression levels of myogenic marker genes. Interestingly ATGL silenced cells tend to express even higher levels of myogenic marker genes than the controls, suggesting a stronger differentiation commitment. One possible explanation could be that there was enough residual ATGL activity, since the knockdown was not 100%. This could be sufficient to provide the cells with enough lipids to maintain a certain signaling status, adequate for the essential processes. Moreover, since there was no nutritional stress, due to frequent glucose supply, cells weren't relying on FFAs as energy source. In line with the symptoms described in the literature, knockdown cells markedly accumulated lipids due to

[2] Matthijs Hesselink, Diabetes and Metabolism Research Group, Maastricht University, Netherlands

decreased TG hydrolysis. As we observed no increase in adipocyte marker genes in ATGL silenced myocytes we assume that no transdifferentiation into adipocytes occurred.

Besides myogenic differentiation properties, we also analyzed adipogenic differentiation characteristics to check whether ATGL silenced myoblasts are more committed to adipocyte differentiation. As reported in the literature, C2C12 cells increased adipocyte marker levels after we applied the adipogenic protocol. Gene expression of adipocyte marker genes peaked at day 4, when the shift towards maintenance media was performed. The change towards a media with less stimulating compounds could explain why marker levels decreased slightly the following days. Nonetheless, adipocytes were formed during the process, indicated by elevated levels of white adipocyte markers SCD1 and aP2/FABP4. Remarkably, our data showed that both surveilled clones differed during adipogenic differentiation. While clone 774 expressed higher levels of the marker genes than the control, indicating higher adipogenic differentiation potency, clone 777 exhibited reduced expression of adipocyte marker genes. Maybe this is due to differences in ATGL transcript level. As suspected for the myogenic differentiation, it is possible that the remaining ATGL activity is sufficient for cellular processes in the presence of glucose as energy metabolite. It is also feasible, that the lentiviral integration disrupted genes that affect differentiation. Furthermore, it is possible that the introduced siRNA is not specific for ATGL, resulting in the degradation of different mRNA targets. Although some adipocytes were formed during adipogenic differentiation, most cells still followed the myogenic lineage as evidenced by high expression levels of myogenic markers. Moreover, morphological evaluation of the cultures showed predominantly myogenic differentiated myotubes. Therefore, we conclude that the decrement of ATGL doesn’t lead to myoblast transdifferentiation towards adipocytes.

One major reason why primary human satellite cells but not murine C2C12 cells show impaired differentiation upon ATGL deficiency could be due to species specific differences in the role of ATGL in muscle differentiation. Moreover, C2C12 cells are immortalized cells that may gained several mutations during propagation which may affect their differentiation properties. Furthermore, C2C12 cells are already committed to myoblasts, making it impossible to study the early differentiation phase from satellite cells to myoblasts.

In order to investigate the lack of ATGL ex vivo in primary satellite cells of mouse muscles, we established an isolation protocol. Marker analysis combined with morphological examination showed that we could successfully isolate and differentiate satellite cells from wild type mice. As described in the literature, the cells were refractive, displayed a roundish shape and expressed

the canonical satellite cell marker Pax7. Furthermore, Pax7 expression decreased upon differentiation, confirming the cells to be satellite cells. During the performed myogenic and adipogenic differentiation MHC2B gene expression rose heavily, although the increase was more pronounced under myogenic conditions. This indicates that most cells entered the myogenic lineage, even upon the administration of adipogenic media. Morphological examination revealed characteristic myotube formation under myogenic- and adipogenic conditions. The drop of MyoD gene expression levels could be due to fact, that cells were already committed to the myogenic lineage when the analysis was performed, owing to higher cell density. Hence, the advanced differentiation status of the cultured cells could explain why they dropped MyoD expression to basal levels and why they preferably entered the myogenic lineage. Nonetheless, the transdifferentiation to adipocytes upon adipogenic induction occurred to some extent, since gene expression of aP2/FABP4 was notably higher when adipogenic induction media was applied. The pattern of ATGL expression matched the trend seen in C2C12 cells. In both cell types, ATGL expression increased upon differentiation. Conversely, this raised the question, whether the lack of ATGL influences the differentiation.

As mentioned before, unpublished data from the group of Matthijs Hesselink suggested defective muscle cell differentiation in the absence of ATGL in patients suffering from NLSDM. We intended to verify these results in satellite cells of ATGL knockout mice, but we were not able to isolate significant amounts of cells. One could assume that the isolation was unsuccessful because the mice used for the isolation were overaged. Instead of 4-week-old mice, as used for the wild type cell isolation, the mice were 9 weeks of age. Therefore the possibility exists that satellite cells of older mice had entirely entered the quiescent state, whereas satellite cells in young mice where still proliferating to grow the muscle.

Elderely humans show pronounced symptoms of muscle atrophy impinging their locomotive capabilities. To evaluate whether old mice also display skeletal muscle impairments, providing a model for in vivo studies, we analyzed markers of muscle atrophy in quadriceps femoris muscle of 19-month-old mice. Furthermore, ATGL expression was examined to determine whether its expression level correlates with skeletal muscle health. Contrary to our expectations, old mice showed no signs of muscle damage. Compared to 4-month old mice, neither Ubiquitin ligase expression, nor autophagy marker protein levels increased. In addition, gene expression and protein levels of ATGL were not altered in aged mice, indicating unrestrained lipolysis. In line, TG levels did not differ between young and old mice. This contrasts findings in aged humans where sarcopenia is present. One possible explanation could be that humans reach higher ages

due to developments in the medical- and technological field. Novel therapeutic techniques prolong life expectancy and quality. However, these treatments can't prevent degenerative processes in later decades. Mice probably don't exceed their physiological lifespan to this extent. It is possible that mice also exhibit muscle impairments when their lifespan is artificially prolonged.

Interestingly, Aquilano and colleagues performed a similar study with quite diverging results (79). They could show a severe reduced ATGL expression accompanied by increased levels of damage markers in gastrocnemius/soleus muscles of 80-week-old mice (79). Furthermore, their data implies that the antioxidative response is impaired due to reduced lipid signaling upon ATGL decrement, leading to elevated levels of oxidatively damaged proteins (79).

In contrast to our experiments, Aquilano and colleagues fasted the mice for 7 hours, before the muscles were taken. During fasting ATGL is needed to provide the organism with energy substrates in form of FFA. In fasted mice reduced ATGL activity leads to a nutritional undersupply and mice need to break down their muscles in order to get energy substrates. Moreover, lipid signaling could be impaired due to reduced liberation of lipid ligands. As a consequence thereof, cellular stress could trigger muscular damage in old mice. ATGL gene expression in old mice is probably sufficient under regular physiological circumstances, but fails to cope with the challenges of detrimental conditions as they appear upon longer periods of fasting. We did not fast mice, so they weren't required to adapt ATGL expression in order to generate energy metabolites. The provided nutrition could have prevented the mice from utilizing muscular proteins as energy source. Furthermore, it is possible that enough lipid ligands were produced to maintain the physiological lipid signaling status. Therefore, signs of muscular degeneration did not appear in old mice under non-fasting conditions. Another explanation for the different observations could be that different muscle depots with different characteristics were used in the experiments. However, both depots contained at least 50% type-I fibers expressing ATGL (81; 82).

Since we did not observe muscle degeneration in old mice, we intended to induce the damage by injecting glycerol into gastrocnemius (GC) and tibialis anterior (TA) muscle. The applied protocol was reported to facilitate detrimental processes characterized by the formation of degenerative adipocytes in a measurable quantity (75). When the experiment was performed in wild type mice, GC muscles neither showed increased adipocyte marker gene expression nor signs of TG accumulation. Further histological examination couldn't reveal any adipocyte

development, supporting the notion that fatty degeneration wasn't induced in GC muscles. TA muscles on the other hand showed slightly increased values of adipocyte marker gene expression. Due to the reduced amount of specimen, determination of lipid content was not possible. Therefore, adipocyte marker levels provide the only hint that some adipocytes may have been formed in TA muscle. Owing to the fact that the injections have to be performed manually, the reproducible application into the muscle is challenging. There is no way to know for sure that the given glycerol reached its target in the muscle. It is very likely that more practice would lead to a greater yield of adipocytes.

Since, the experimental procedure would require more optimization, the studies were terminated without testing the protocol in ATGL knockout mice. Therefore we can't draw comparisons between the loss of ATGL and the amount of degeneratively formed adipocytes, which was the primary intend of this experiment.

Taken together, our data indicate that there is no negative impact of reduced ATGL expression on the differentiation of mouse myoblasts towards myotubes. Moreover, we succeeded in establishing a protocol for the isolation of primary muscle cells from mouse muscles. Interestingly we found that old mice do not resemble aged humans with respect to muscle damage, and hence are not suited to study sarcopenia.

7 Abbreviations

APS	ammonium persulfate
ATGL	Adipose triglyceride lipase
BCA	bicinchoninic acid
BSA	bovine serum albumin
CAPS	N-cyclohexyl-3-aminopropanesulfonic acid
cDNA	complementary DNA
ddH_2O	distilled, deionized water
DG	diacylglycerol
DIC	differential interference contrast
DMEM	Dulbecco's Modified Eagle Medium
DMSO	dimethyl sulfoxide
DNA	deoxyribonucleic acid
EDTA	ethylenediaminetetraacetic acid
FAP	Fibro/adipogenic progenitor
FFA	free fatty acid
FCS	fetal calf serum
Fwd	forward
GAPDH	glyceraldehyde 3-phosphate dehydrogenase
GC	gastrocnemius muscle
HSL	Hormone-sensitive lipase
IBMX	3-isobutyl-1-methylxanthine

IMAT	intramuscular adipose tissue
kDa	kilodalton
LD	lipid droplet
MG	monoacylglycerol
MGL	Monoacylglycerol lipase
mRNA	messenger RNA
MyoG	myogenin
PBS	phosphate buffered saline
PCR	polymerase chain reaction
Plin	Perilipin
PPAR	peroxisome proliferator-activated receptors
qRT-PCR	quantitative real-time PCR
Rev	reverse
RNA	ribonucleic acid
rpm	revolutions per minute
SDS	sodium dodecyl sulfate
siRNA	small interfering RNA
TA	tibialis anterior muscle
TEMED	tetra methyl ethylene diamine
TF	transcription factor
TG	triacylglycerol
µ	micro

8 References

1. Lass, A., Zimmerman, R., Oberer, M., and Zechner, R. (2011) Lipolysis - a highly regulated multi-enzyme complex mediates the catabolism of cellular fat stores. *Progress in Lipid Research* **50**, 14-27

2. Tauchi-Sato, K., Ozeki S., Houjou, T., Taguchi, R., Fujimoto, T. (2002) The Surface of Lipid Droplets Is a Phospholipid Monolayer with a Unique Fatty Acid Composition. *THE JOURNAL OF BIOLOGICAL CHEMISTRY* **277**, 44507-12

3. Zweytick, D., Athenstaedt, K., Daum, G. (2000) Intracellular lipid particles of eukaryotic cells. *Biochimica et Biophysica Acta* **1469**, 101-20

4. Brasaemle, D. L. (2007) The perilipin family of structural lipid droplet proteins: stabilization of lipid droplets and control of lipolysis. *The Journal of Lipid Research* **48**, 2547-59

5. Villena, J. A., Roy, S., Sarkadi-Nagy, E., Kim, K. H., Sul, H. S. (2004) Desnutrin, an adipocyte gene encoding a novel patatin domain-containing protein, is induced by fasting and glucocorticoids: ectopic expression of desnutrin increases triglyceride hydrolysis. *The Journal of Biological Chemistry* **279**, 47066-75

6. Kershaw, E. E., Schupp, M., Guan, H. P., Gardner, N. P., Lazar, M. A., Flier, J. S. (2007) PPARgamma regulates adipose triglyceride lipase in adipocytes in vitro and in vivo. *American journal of physiology. Endocrinology and metabolism* **293**, 1736-45

7. Zechner, R., Zimmermann, R., Eichmann, T. O., Kohlwein, S. D., Haemmerle, G., Lass, A., Madeo, F. (2012) FAT SIGNALS - Lipases and Lipolysis in Lipid Metabolism and Signaling. *Cell Metabolism* **15**, 279-91

8. Lass, A., Zimmermann, R., Haemmerle, G., Riederer, M., Schoiswohl, G., Schweiger, M., Kienesberger, P., Strauss, J. G., Gorkiewicz, G., Zechner, R. (2006) Adipose triglyceride lipase-mediated lipolysis of cellular fat stores is activated by CGI-58 and defective in Chanarin-Dorfman Syndrome. *Cell Metab* **3**, 309-19

9. Lefèvre, C., Jobard, F., Caux, F., Bouadjar, B., Karaduman, A., Heilig, R., Lakhdar, H., Wollenberg, A.,Verret, J. L., Weissenbach, J., Ozgüc, M., Lathrop, M., Prud'homme, J. F., Fischer, J. (2001) Mutations in CGI-58, the gene encoding a new protein of the esterase/lipase/thioesterase subfamily, in Chanarin-Dorfman syndrome. *American Journal of Human Genetics* **69**, 1002-12

10. Yang, X., Lu, X., Lombès, M., Rha, G. B., Chi, Y. I., Guerin, T. M., Smart, E. J., Liu, J. (2010) The G(0)/G(1) switch gene 2 regulates adipose lipolysis through association with adipose triglyceride lipase. *Cell Metababolism* **11**, 194-205

11. Lu, X., Yang, X., Liu, J. (2010) Differential control of ATGL-mediated lipid droplet degradation by CGI-58 and G0S2. *Cell Cycle* **9**, 2719-25

12. Yamaguchi, T., Omatsu, N., Matsushita, S., Osumi, T. (2004) CGI-58 interacts with perilipin and is localized to lipid droplets. Possible involvement of CGI-58 mislocalization in Chanarin-Dorfman syndrome. *The Journal of Biological Chemistry* **279**, 30490-7

13. Granneman, J. G., Moore, H. P., Krishnamoorthy, R., Rathod, M. (2009) Perilipin controls lipolysis by regulating the interactions of AB-hydrolase containing 5 (Abhd5) and adipose triglyceride lipase (Atgl). *The Journal of Biological Chemistry* **284**, 34538-44

14. Miyoshi, H., Perfield, J. W. 2nd., Souza, S. C., Shen, W. J., Zhang, H. H., Stancheva, Z. S., Kraemer, F. B., Obin, M. S., Greenberg, A. S. (2007) Control of adipose triglyceride lipase action by serine 517 of perilipin A globally regulates protein kinase A-stimulated lipolysis in adipocytes. *The Journal of Biological Chemistry* **282**, 996-1002

15. Strålfors, P., Belfrage, P. (1983) Phosphorylation of hormone-sensitive lipase by cyclic AMP-dependent protein kinase. *The Journal of Biological Chemistry* **258**, 15146-52

16. Miyoshi, H., Souza, S. C., Zhang, H. H., Strissel, K. J., Christoffolete, M. A., Kovsan, J., Rudich, A., Kraemer, F. B., Bianco, A. C., Obin, M. S., Greenberg, A. S. (2006) Perilipin promotes hormone-sensitive lipase-mediated adipocyte lipolysis via phosphorylation-dependent and -independent mechanisms. *The Journal of Biological Chemistry* **281**, 15837-44

17. Shen, W. J., Patel, S., Miyoshi, H., Greenberg, A. S., Kraemer, F. B. (2009) Functional interaction of hormone-sensitive lipase and perilipin in lipolysis. *The Journal of Lipid Research* **50**, 2306-13

18. Wang, H., Hu, L., Dalen, K., Dorward, H., Marcinkiewicz, A., Russell, D., Gong, D., Londos, C., Yamaguchi, T., Holm, C., Rizzo, M. A., Brasaemle, D., Sztalryd, C. (2009) Activation of hormone-sensitive lipase requires two steps, protein phosphorylation and binding to the PAT-1 domain of lipid droplet coat proteins. *The Journal of Biological Chemistry* **284**, 32116-25

19. Wolins, N. E., Quaynor, B. K., Skinner, J. R., Tzekov, A., Croce, M. A., Gropler, M. C., Varma, V., Yao-Borengasser., A., Rasouli, N., Kern, P. A., Finck, B. N., Bickel, P.E. (2006) OXPAT/PAT-1 is a PPAR-induced lipid droplet protein that promotes fatty acid utilization. *Diabetes* **55**, 3418-28

20. Granneman, J. G., Moore, H. P., Mottillo, E. P., Zhu, Z., Zhou, L. (2011) Interactions of perilipin-5 (Plin5) with adipose triglyceride lipase. *The Journal of Biological Chemistry* **286**, 5126-35

21. Granneman, J. G., Moore, H. P., Mottillo, E. P., Zhu, Z. (2009) Functional interactions between Mldp (LSDP5) and Abhd5 in the control of intracellular lipid accumulation. *The Journal of Biological Chemistry* **284**, 3049-57

22. Watt, M. J., Holmes, A. G., Pinnamaneni, S. K., Garnham, A. P., Steinberg, G. R., Kemp, B. E., Febbraio, M. A. (2006) Regulation of HSL serine phosphorylation in skeletal muscle and adipose tissue. *American journal of physiology. Endocrinology and metabolism* **290**, E500-8.

23. Haemmerle, G., Moustafa, T., Woelkart, G., Büttner, S., Schmidt, A., van de Weijer, T., Hesselink, M., Jaeger, D., Kienesberger, P. C., Zierler, K., Schreiber, R., Eichmann, T., Kolb, D., Kotzbeck, P., Schweiger, M., Kumari, M., Eder, S., Schoiswohl, G., Wongsiriroj, N., Pollak, N. M., Radner, F. P., Preiss-Landl, K., Kolbe, T., Rülicke, T., Pieske, B., Trauner, M., Lass, A., Zimmermann, R., Hoefler, G., Cinti, S., Kershaw, E. E., Schrauwen, P., Madeo, F., Mayer, B., Zechner, R. (2011) ATGL-mediated fat catabolism regulates cardiac mitochondrial function via PPAR-α and PGC-1. *Nature Medicine* **17**, 1076-85

24. Schreiber, R., Hofer, P., Taschler, U., Voshol, P. J., Rechberger, G. N., Kotzbeck, P., Jaeger, D., Preiss-Landl, K., Lord, C. C., Brown, J. M., Haemmerle, G., Zimmermann, R., Vidal-Puig, A., Zechner, R. (2015) Hypophagia and metabolic adaptations in mice with defective ATGL-mediated lipolysis cause resistance to HFD-induced obesity. *Proceedings of the National Academy of Sciences* **112**, 13850-5

25. Zimmermann, R., Strauss, J. G., Haemmerle, G., Schoiswohl, G., Birner-Gruenberger, R., Riederer, M., Lass, A., Neuberger, G., Eisenhaber, F., Hermetter, A., Zechner, R. (2004) Fat mobilization in adipose tissue is promoted by adipose triglyceride lipase. *Science* **306**, 1383-6

26. Jenkins, C. M., Mancuso, D. J., Yan, W., Sims, H. F., Gibson, B., Gross, R. W. (2004) Identification, cloning, expression, and purification of three novel human calcium-independent phospholipase A2 family members possessing triacylglycerol lipase and acylglycerol transacylase activities. *The Journal of Biological Chemistry* **279**, 48968-75

27. Wilson, P. A., Gardner, S. D., Lambie, N. M., Commans, S. A., Crowther, D. J. (2006) Characterization of the human patatin-like phospholipase family. *The Journal of Lipid Research* **47**, 1940-9

28. Notari, L., Baladron, V., Aroca-Aguilar, J. D., Balko, N., Heredia, R., Meyer, C., Notario, P. M., Saravanamuthu, S., Nueda, M. L., Sanchez-Sanchez, F., Escribano, J., Laborda, J., Becerra, S. P. (2006) Identification of a lipase-linked cell membrane receptor for pigment epithelium-derived factor. *The Journal of Biological Chemistry* **281**, 38022-37

29. Rydel, T. J., Williams, J. M., Krieger, E., Moshiri, F., Stallings, W. C., Brown, S. M., Pershing, J. C., Purcell, J. P., Alibhai, M. F. (2003) The crystal structure, mutagenesis, and activity studies reveal that patatin is a lipid acyl hydrolase with a Ser-Asp catalytic dyad. *Biochemistry* **42**, 6696-708

30. Smirnova, E., Goldberg, E. B., Makarova, K. S., Lin, L., Brown, W. J., Jackson, C. L. (2006) ATGL has a key role in lipid droplet/adiposome degradation in mammalian cells. *EMBO Reports* **7**, 106-13

31. Schweiger, M., Schoiswohl, G., Lass, A., Radner, F. P., Haemmerle, G., Malli, R., Graier, W., Cornaciu, I., Oberer, M., Salvayre, R., Fischer, J., Zechner, R., Zimmermann, R. (2008) The C-terminal region of human adipose triglyceride lipase affects enzyme activity and lipid droplet binding. *The Journal of Biological Chemistry* **283**, 17211-20

32. Kobayashi, K., Inoguchi, T., Maeda, Y., Nakashima, N., Kuwano, A., Eto, E., Ueno, N., Sasaki, S., Sawada, F., Fujii, M., Matoba, Y., Sumiyoshi, S., Kawate, H., Takayanagi, R. (2008) The lack of the C-terminal domain of adipose triglyceride lipase causes neutral lipid storage disease through impaired interactions with lipid droplets. *The Journal of Clinical Endocrinology and Metabolism* **93**, 2877-84

33. Lake, A. C., Sun, Y., Li, J. L., Kim, J. E., Johnson, J. W., Li, D., Revett, T., Shih, H. H., Liu, W., Paulsen, J. E., Gimeno, R. E. (2005) Expression, regulation, and triglyceride hydrolase activity of Adiponutrin family members. *The Journal of Lipid Research* **46**, 2477-87

34. Kershaw, E. E., Hamm, J. K., Verhagen, L. A., Peroni, O., Katic, M., Flier, J. S. (2006) Adipose triglyceride lipase: function, regulation by insulin, and comparison with adiponutrin. *Diabetes* **55**, 148-57

35. Haemmerle, G., Lass, A., Zimmermann, R., Gorkiewicz, G., Meyer, C., Rozman, J., Heldmaier, G., Maier, R., Theussl, C., Eder, S., Kratky, D., Wagner, E. F., Klingenspor, M., Hoefler, G., Zechner, R. (2006) Defective lipolysis and altered energy metabolism in mice lacking adipose triglyceride lipase. *Science* **312**, 734-7

36. Schweiger, M., Lass, A., Zimmermann, R., Eichmann, T. O., Zechner, R. (2009) Neutral lipid storage disease: genetic disorders caused by mutations in adipose triglyceride lipase/PNPLA2 or CGI-58/ABHD5. *American journal of physiology. Endocrinology and metabolism* **297**, E289-96

37. Igal, R. A., Rhoads, J. M., Coleman, R. A. (1997) Neutral lipid storage disease with fatty liver and cholestasis. *Journal of Pediatric Gastroenterology and Nutrition* **25**, 541-7

38. Chanarin, I., Patel, A., Slavin, G., Wills, E. J., Andrews, T. M., Stewart, G. (1975) Neutral-lipid storage disease: a new disorder of lipid metabolism. *British medical journal* **1**, 553-5

39. Jordans, G. H. (1953) The familial occurrence of fat containing vacuoles in the leukocytes diagnosed in two brothers suffering from dystrophia musculorum progressiva (ERB.). *Acta Medica Scandinavica* **145**, 419-23

40. Fischer, J., Lefèvre, C., Morava, E., Mussini, J. M., Laforêt, P., Negre-Salvayre, A., Lathrop, M., Salvayre, R. (2007) The gene encoding adipose triglyceride lipase (PNPLA2) is mutated in neutral lipid storage disease with myopathy. *Nature Genetics* **39**, 28-30

41. Pasanisi, M. B., Missaglia, S., Cassandrini, D., Salerno, F., Farina, S., Andreini, D., Agostoni, P., Morandi, L., Mora, M., Tavian, D. (2016) Severe cardiomyopathy in a young patient with complete deficiency of adipose triglyceride lipase due to a novel mutation in PNPLA2 gene. *International Journal of Cardiology* **207**, 165-7

42. Missaglia, S., Tasca, E., Angelini, C., Moro, L., Tavian, D. (2015) Novel missense mutations in PNPLA2 causing late onset and clinical heterogeneity of neutral lipid storage disease with myopathy in three siblings. *Molecular Genetics and Metabolism* **115**, 110-7

43. Akiyama, M., Sakai, K., Ogawa, M., McMillan, J. R., Sawamura, D., Shimizu, H. (2007) Novel duplication mutation in the patatin domain of adipose triglyceride lipase (PNPLA2) in neutral lipid storage disease with severe myopathy. *Muscle Nerve* **36**, 856-9

44. Kaneko, K., Kuroda, H., Izumi, R., Tateyama, M., Kato, M., Sugimura, K., Sakata, Y., Ikeda, Y., Hirano, K., Aoki, M. (2014) A novel mutation in PNPLA2 causes neutral lipid storage disease with myopathy and triglyceride deposit cardiomyovasculopathy: a case report and literature review. *Neuromuscular Disorders* **24**, 634-41

45. Hirano, K., Tanaka, T., Ikeda, Y., Yamaguchi, S., Zaima, N., Kobayashi, K., Suzuki, A., Sakata, Y., Sakata, Y., Kobayashi, K., Toda, T., Fukushima, N., Ishibashi-Ueda, H., Tavian, D., Nagasaka, H., Hui, S. P., Chiba, H., Sawa, Y., Hori, M. (2014) Genetic mutations in adipose triglyceride lipase and myocardial up-regulation of peroxisome proliferated activated receptor-γ in patients with triglyceride deposit cardiomyovasculopathy. *Biochemical and Biophysical Research Communications* **443**, 574-9

46. Massa, R., Pozzessere, S., Rastelli, E., Serra, L., Terracciano, C., Gibellini, M., Bozzali, M., Arca, M. (2016) Neutral lipid-storage disease with myopathy and extended phenotype with novel PNPLA2 mutation. *Muscle & Nerve* **53**, 644-8

47. Frontera, W. R., Ochala, J. (2015) Skeletal muscle: a brief review of structure and function. *Calcified Tissue International* **96**, 183-95

48. Snijders, T., Nederveen, J. P., McKay, B, R., Joanisse, S., Verdijk, L. B., van Loon, L. J., Parise, G. (2015) Satellite cells in human skeletal muscle plasticity. *Frontiers in physiology* **6**, 283

49. Yin, H., Price, F., Rudnicki, M. A. (2013) Satellite cells and the muscle stem cell niche. *Physiological Reviews* **93**, 23-67

50. Wolfe, R. R. (2006) The underappreciated role of muscle in health and disease. *The American Journal of Clinical Nutrition* **84**, 475-82

51. Mauro, A. (1961) Satellite cell of skeletal muscle fibers. *The Journal of Biophysical and Biochemical Cytology* **9**, 493-5

52. Seale, P., Sabourin, L. A., Girgis-Gabardo, A., Mansouri, A., Gruss, P., Rudnicki, M. A. (2000) Pax7 is required for the specification of myogenic satellite cells. *Cell* **102**, 777-86

53. Olguin, H. C., Yang, Z., Tapscott, S. J., Olwin, B. B. (2007) Reciprocal inhibition between Pax7 and muscle regulatory factors modulates myogenic cell fate determination. *The Journal of cell biology* **177**, 769-79

54. Tamaki, T., Akatsuka, A., Yoshimura, S., Roy, R. R., Edgerton, V. R. (2002) New fiber formation in the interstitial spaces of rat skeletal muscle during postnatal growth. *Journal of Histochemistry & Cytochemistry* **50**, 1097-111

55. Bischoff, R. (1986) A satellite cell mitogen from crushed adult muscle. *Developmental biology* **115**, 140-7

56. Francetic, T., Li, Q. (2011) Skeletal myogenesis and Myf5 activation. *Transcription* **2**, 109-14

57. Beauchamp, J. R., Heslop, L., Yu, D. S., Tajbakhsh, S., Kelly, R. G., Wernig, A., Buckingham, M. E., Partridge, T. A., Zammit, P. S. (2000) Expression of CD34 and Myf5 defines the majority of quiescent adult skeletal muscle satellite cells. *The Journal of cell biology* **151**, 1221-34

58. Smith C. K. 2nd., Janney, M. J., Allen, R. E. (1994) Temporal expression of myogenic regulatory genes during activation, proliferation, and differentiation of rat skeletal muscle satellite cells. *Journal of cellular physiology* **159**, 379-85

59. Cornelison, D. D., Wold, B. J. (1997) Single-cell analysis of regulatory gene expression in quiescent and activated mouse skeletal muscle satellite cells. *Developmental biology* **191**, 270-83

60. Asakura, A., Komaki, M., Rudnicki, M. (2001) Muscle satellite cells are multipotential stem cells that exhibit myogenic, osteogenic, and adipogenic differentiation. *Differentiation; research in biological diversity* **68**, 245-53

61. Joe, A. W., Yi. L., Natarajan, A., Le Grand, F., So, L., Wang, J., Rudnicki, M. A., Rossi, F. M. (2010) Muscle injury activates resident fibro/adipogenic progenitors that facilitate myogenesis. *Nature cell biology* **12**, 153-63

62. Uezumi, A., Fukada, S., Yamamoto, N., Takeda, S., Tsuchida, K. (2010) Mesenchymal progenitors distinct from satellite cells contribute to ectopic fat cell formation in skeletal muscle. *Nature cell biology* **12**, 143-52

63. Liu, W., Liu, Y., Lai, X., Kuang, S. (2012) Intramuscular adipose is derived from a non-Pax3 lineage and required for efficient regeneration of skeletal muscles. *Developmental biology* **361**, 27-38

64. Yaffe, D., Saxel, O. (1977) Serial passaging and differentiation of myogenic cells isolated from dystrophic mouse muscle. *Nature* **270**, 725-7

65. Blau, H. M., Pavlath, G. K., Hardeman, E. C., Chiu, C. P., Silberstein, L., Webster, S. G., Miller, S. C., Webster, C. (1985) Plasticity of the differentiated state. *Science* **230**, 758-66

66. Lin, Y., Zhao, Y., Li, R., Gong, J., Zheng, Y., Wang, Y. (2014) PGC-1α is associated with C2C12 Myoblast differentiation. *Central European Journal of Biology* **9**, 1030-36

67. Tobon, A. (2013) Metabolic myopathies. *Continuum (Minneapolis, Minn.)* **19**, 1571-97

68. Atluri, R. B. (2016) Inflammatory Myopathies. *Missouri Medicine* **113**, 127-30

69. Pasnoor, M., Barohn, R. J., Dimachkie, M. M. (2014) Toxic myopathies. *Neurologic Clinics* **32**, 647-70

70. Shieh, P. B. (2013) Muscular dystrophies and other genetic myopathie. *Neurologic Clinics* **31**, 1009-29

71. Yiu, E. M., Kornberg, A. J. (2015) Duchenne muscular dystrophy. *Journal of Paediatrics and Child Health* **51**, 759-64

72. Santilli, V., Bernetti, A., Mangone, M., Paoloni, M. (2014) Clinical definition of sarcopenia. *Clinical Cases in mineral and bone metabolism* **11**, 177-80

73. Vettor, R., Milan, G., Franzin, C., Sanna, M., De Coppi, P., Rizzuto, R., Federspil, G. (2009) The origin of intermuscular adipose tissue and its pathophysiological implications. *American journal of physiology. Endocrinology and metabolism* **297**, E987-98

74. Sciorati, C., Clementi, E., Manfredi, A. A., Rovere-Querini, P. (2015) Fat deposition and accumulation in the damaged and inflamed skeletal muscle: cellular and molecular players. *Cellular and Molecular Life Sciences* **72**, 2135-56

75. Pisani, D. F., Bottema, C. D., Butori, C., Dani, C., Dechesne, C. A. (2010) Mouse model of skeletal muscle adiposity: a glycerol treatment approach. *Biochemical and Biophysical Research Communications* **396**, 767-73

76. Jocken, J. W., Smit, E., Goossens, G. H., Essers, Y. P., van Baak, M. A., Mensink, M., Saris, W. H., Blaak, E. E. (2008) Adipose triglyceride lipase (ATGL) expression in human skeletal muscle is type I (oxidative) fiber specific. *Histochemistry and Cell Biology* **129**, 535-8

77. Angelini, C. (2015) Spectrum of metabolic myopathies. *Biochimica et Biophysica Acta* **1852**, 615-21

78. Reilic, P., Horvath, R., Krause, S., Schramm, N., Turnbull, D. M., Trenell, M., Hollingsworth, K. G., Gorman, G. S., Hans, V. H., Reimann, J., MacMillan, A., Turner, L., Schollen, A., Witte, G., Czermin, B., Holinski-Feder, E., Walter, M. C., Schoser, B., Lochmüller, H. (2011) The phenotypic spectrum of neutral lipid storage myopathy due to mutations in the PNPLA2 gene. *Journal of Neurology* **258**, 1987-97

79. Aquilano, K., Baldelli, S., La Barbera, L., Lettieri Barbato, D., Tatulli, G., Ciriolo, M. R. (2016) Adipose triglycerides lipase decrement affects skeletal muscle homeostasis during aging through FAs-PPARα-PGC-1α antioxidant response. *Oncotarget* **26**, 23019-23032

80. Sraer, J. D., Moulonguet-Doleris, L., Delarue, F., Sraer, J., Ardaillou, R. (1981) Prostaglandin synthesis by glomeruli isolated from rats with glycerol-induced acute renal failure. *Circulation Research* **49**, 775-83

81. Edgerton, V. R., Smith, J. L., Simpson, D. R. (1975) Muscle fibre type populations of human leg muscles. *The Histochemical Journal* **7**, 259-66

82. Staron, R. S., Hagerman, F. C., Hikida, R. S., Murray, T. F., Hostler, D. P., Crill, M. T., Ragg, K. E., Toma, K. (2000) Fiber type composition of the vastus lateralis muscle of young men and women. *Journal of Histochemistry & Cytochemistry* **48**, 623-9

9 List of figures